On the Nature of Alkali Ion−Water Interactions: Insights from Many-Body Representations and Density Functional Theory. II.

Colin K. Egan,*,† Brandon B. Bizzarro,† Marc Riera,† and Francesco Paesani*,†,‡,¶

†*Department of Chemistry and Biochemistry, University of California San Diego, La Jolla, California 92093, United States*

‡*Materials Science and Engineering, University of California San Diego, La Jolla, California 92093, United States*

¶*San Diego Supercomputer Center, University of California San Diego, La Jolla, California 92093, United States*

E-mail: ckegan@ucsd.edu; fpaesani@ucsd.edu

Abstract

Interaction energies of alkali ion−water dimers, $M^+(H_2O)$, and trimers, $M^+(H_2O)_2$, with M = Li, Na, K, Rb, Cs, are investigated using various many-body potential energy functions, and exchange correlation functionals selected across the hierarchy of density functional theory approximations. Analysis of interaction energy decompositions indicates that close range interactions such as Pauli repulsion, charge transfer, and charge penetration must be captured in order to reproduce accurate interaction energies. In particular, it is found that simple classical polarizable models must be supplemented with dedicated terms which account for these close range interactions

in order to achieve chemical accuracy across configuration space. It is also found that the XC functionals mostly differ from each other in their Pauli repulsion + Dispersion energies, and hence benefit from the inclusion of nonlocal terms such as Hartree-Fock exchange and dependence on the electronic kinetic energy density in order to reproduce the interactions that contribute to this term, namely Pauli repulsion and (intermediate-range) dispersion. As a continuation of the analysis performed in J. Chem. Theory Comput. 2019, 15, 2983, we make comparisons between findings for alkali ion−water interactions with those for halide−water interactions.

1 Introduction

Molecular dynamics (MD) simulations allow for the calculation of molecular-scale properties of chemical systems that are difficult, or currently impossible, to obtain through experimental means.[1–9] As of today, the primary difficulty in performing MD simulations is solving the Schrödinger equation for the electronic degrees of freedom[10] which provides the potential energy surface (PES).[11] Within the Born-Oppenheimer approximation, the most accurate methods for calculating the PESs, such as the configuration interaction and its approximations such as the coupled cluster hierarchy,[11,12] are prohibitively expensive[13] for condensed phase systems in periodic boundary conditions, which may contain thousands of electrons.

One of the most efficient approaches to calculating approximate PESs for MD simulations is the use of analytical potential energy functions (PEFs),[14,15] commonly known as force fields (FFs), wherein the electronic degrees of freedom are effectively integrated-out. The efficiency comes at a cost, however, since the complicated nature of the electronic structure of molecular systems requires that the comparatively-simple analytic PEFs be tailored specifically to the system of interest, often requiring that each atom be assigned a unique identity that must be preserved during an MD simulation.

Alternatively, density functional theory (DFT) allows for the calculation of PESs for MD simulations through an explicit treatment of the electron density, thus circumventing the

need for reparametrization for each system of interest. DFT requires a much greater cost than analytic PEFs, but is tractable for simulations of relatively small systems, unlike the configuration interaction or coupled cluster methods. However, it has been shown[16–20] that the approximate exchange-correlation (XC) functionals used in DFT simulations of aqueous systems can yield PESs that are much less accurate than those produced by analytic PEFs.

We previously conducted an analysis of the energy decompositions of a number of PEFs and popular XC functionals in calculating halide ion−water interaction energies[20] to identify interaction components that are necessary to achieve sufficient accuracy, and to identify limitations of the tested models. Energy decompositions of the PEFs are easily calculated since the three tested models (AMOEBA,[21,22] TTM-nrg,[23,24] and MB-nrg[18,19]) are constructed as a sum of contributions arising from specific interactions, such as permanent electrostatics (ELEC), polarization (POL), Pauli repulsion (PAULI), and dispersion (DISP) (where the PAULI and DISP terms are often represented as a single term, which we refer to as "Pauli+Disp," such as the Lennard-Jones and Buckingham potentials), along with terms due to intramolecular distortion energies (bond stretches, angle bends, dihedrals, etc.) which we are not concerned with here.[25] Energy decompositions of the XC functionals were computed using the 2$^{\text{nd}}$ generation absolutely localized molecular orbital energy decomposition analysis (ALMO-EDA) method,[26,27] which decomposes an interaction energy calculated with a given functional into terms due to ELEC, PAULI, DISP, POL and charge transfer (CT).[26–30] It should be noted that in order to keep all analysis consistent, we only discuss the sum of PAULI + DISP = Pauli+Disp energies for both the PEFs and the XC functionals. Despite the fact that these specific interaction terms are not observable quantities,[31,32] and, therefore, energy decompositions of XC functionals are not uniquely-defined, ALMO-EDA was developed to satisfy a number of properties,[20,28] which allows for qualitative comparisons between the descriptions of intermolecular interactions produced by a survey of functionals.[20]

In our analysis of halide−water energy decompositions, it was found that close range interactions such as CT and charge penetration posed the greatest difficulties for the PEFs

that do not include dedicated terms to correct for these effects, while the tested XC functionals displayed greatly-varying accuracies, but were for the most part distinguished from each other in their Pauli+Disp energy terms, and to a lesser extent, in their CT energies. In particular, we found that the MB-nrg PEFs performed better, on average, than all other models (among both the PEFs and the XC functionals), as a result of the balanced treatment of long-range interactions—which are effectively captured with classical representations of ELEC, POL, and DISP terms—with the more complicated close-range interactions where CT and PAULI interactions become significant, and the simple classical long-range representations break down (e.g., CP effects that cannot be captured by damped atomic point charges). The accuracy of the MB-nrg PEFs is achieved through the use of permutationally invariant polynomials[33] (PIPs) fitted to large sets of two-body (2B) and three-body (3B) energies calculated at the coupled cluster level of theory with single, double, and perturbative triple excitations (CCSD(T))[34,35] which act as close range "quantum corrections" to underlying long-range classical potentials which include long-range, system-wide polarization.[18–20] Additionally, it was found that the inclusion of nonlocal terms such as Hartree-Fock exchange (in hybrid functionals), as well as terms dependent on the kinetic energy density (in meta-GGAs) in XC functionals had significant effects on the close-range CT and Pauli+Disp interactions. However, it was also found that Hartree-Fock exchange on its own can be insufficient to improve interaction energies, for example the PBE0 $F^-(H_2O)$ 2B energy was found to deviate from the CCSD(T)-F12b reference energy more than the PBE 2B energy, despite the use of Hartree-Fock exchange.

Here, we extend the analysis of interaction energy decompositions to alkali ion−water interactions as described by various analytical PEFs and XC functionals, paying particular attention to comparisons with analogous results reported in Ref. 20 for halide−water interactions. Specifically, we find that as was the case for halide−water interactions, analytical PEFs entirely based on classical representations of the alkali ion−water interactions have trouble reproducing close-range effects, and that quantum corrections (such as those

from PIPs) can significantly improve accuracy. Furthermore, we find that the MB-nrg[18,19] PEFs yield, on average, the most accurate 2B and 3B energies for alkali ion−water systems among all PEFs and XC functionals tested in this study. We find some differences in trends of energy decompositions of XC functionals for alkali ion−water interactions compared to those for halide−water interactions, but again find that nonlocal terms in XC functionals are needed to reproduce the correct Pauli+Disp energies. In particular, comparisons of Pauli+Disp energies of GGAs, meta-GGAs, hybrid GGAs, and hybrid meta-GGAs suggest that differences in Pauli+Disp energies may be due in part to the ability or inability to capture intermediate-range dispersion interactions. Additionally, through a comparison of alkali ion−water and halide−water Pauli+Disp energies, we identify that the delocalization error[36–38] leads to spurious Pauli repulsion, further deteriorating Pauli+Disp energies of functionals that do not contain sufficient nonlocal character.

2 Theoretical and Computational Methodology

2.1 Electronic structure calculations

$M^+(H_2O)$ and $M^+(H_2O)_2$ (M = Li, Na, K, Rb, Cs) cluster structures were obtained from MP2[39,40] geometry optimizations using the aug-cc-pVTZ basis set[41,42] for water, the cc-pwCVTZ basis set[43] for Li and Na, and the cc-pwCVTZ-PP basis set[44] for K, Rb, and Cs using the ECP10MDF, ECP28MDF, and ECP46MDF effective core potentials, respectively.[45] A threshold of 1.0×10^{-6} a.u., a step size of 1.0×10^{-6} a.u., and a gradient precision of 1.0×10^{-8} a.u. were used in all optimizations.

2B scans of each alkali ion along the water H−O−H bisector were performed by optimizing the water monomer at the RI-MP2[46,47] level of theory with the aug-cc-pVTZ basis set, initially placing each ion, except for Li^+, 1.5 Å away from the water-oxygen (Li^+ was initially placed 1.25 Å away from the oxygen), coplanar with the water molecule, on the other side of the water-hydrogens (Figure 1). Each ion was displaced along the water bisector

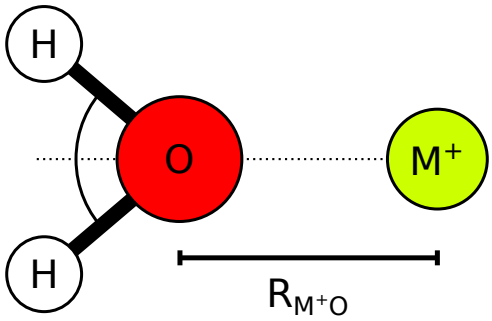

Figure 1: Schematic representation of the geometry used in the scans along the R_{M^+O} distance carried out for each of the four $M^+(H_2O)$ dimers, with M = Li, Na, K, Rb, Cs. The ion remains in the plane of the water molecule.

(in the plane) up to 5.0 Å from the oxygen in 0.1 Å increments.

Reference interaction energies were computed at the CCSD(T)[34,35] level of theory in the complete basis set (CBS) limit using a two-point extrapolation[48] with the aug-cc-pVTZ and aug-cc-pVQZ basis sets for O and H, the cc-pwCVTZ and cc-pwCVQZ basis sets for Li and Na, and the cc-pwCVTZ-PP and cc-pwCVQZ-PP basis sets for K, Rb, and Cs, using the ECP10MDF, ECP28MDF, and ECP46MDF effective core potentials, respectively. In all the calculations, the valence electrons were correlated for O and H, while for the metals, the $n-1$ valence shell was also correlated since there are no electrons in the positively charged cation. All optimizations and energy calculations were performed using MOLPRO 2015.1.[49]

2.2 The AMOEBA force field

The Atomic Multipole Optimized Energetics for Biomolecular Applications (AMOEBA) is a polarizable FF commonly used in MD simulations.[21,22,50–53] A thorough description of the AMOEBA FF can be found in the original references.[14,21] The AMOEBA functional form for the total interaction energy is expressed as:

$$V_{\mathrm{INT}}^{\mathrm{AMOEBA}} = V_{\mathrm{ELEC}}^{\mathrm{AMOEBA}} + V_{\mathrm{POL}}^{\mathrm{AMOEBA}} + V_{\mathrm{Pauli+Disp}}^{\mathrm{AMOEBA}} \quad (1)$$

The AMOEBA FF employs classical Coulombic equations to describe the permanent electrostatic potential energy, $V_{\mathrm{ELEC}}^{\mathrm{AMOEBA}}$, using atom-centered point multipoles (monopoles through the quadrupole) calculated via distributed multipole analysis (DMA) from MP2/aug-cc-pVTZ.[21] $V_{\mathrm{POL}}^{\mathrm{AMOEBA}}$ is treated explicitly, including self-consistent atom-centered induced point dipoles. Atomic isotropic polarizabilities are derived from fits to experimental data.[14,21] To avoid overpolarization at close range, a Thole-type electrostatic damping scheme, with exponential-3 damping is used in $V_{\mathrm{POL}}^{\mathrm{AMOEBA}}$.[21,54] None of the terms in $V_{\mathrm{ELEC}}^{\mathrm{AMOEBA}}$ are damped.

The remaining energy contribution, $V_{\mathrm{Pauli+Disp}}^{\mathrm{AMOEBA}}$, is modeled with the buffered 14-7 potential[55] to capture close-range pairwise additive interactions and can be decomposed into terms which mainly correspond to Pauli-repulsion and London dispersion:

$$\begin{aligned} V_{\mathrm{Pauli+Disp}}^{\mathrm{AMOEBA}} &= \sum_{i<j} \epsilon_{ij} \left(\frac{1+\delta}{\rho_{ij}+\delta}\right)^7 \left(\frac{1+\gamma}{\rho_{ij}^7+\gamma} - 2\right) \\ &= \sum_{i<j} \epsilon_{ij} \left(\frac{1+\delta}{\rho_{ij}+\delta}\right)^7 \left(\frac{1+\gamma}{\rho_{ij}^7+\gamma}\right) - 2\epsilon_{ij} \left(\frac{1+\delta}{\rho_{ij}+\delta}\right)^7 \end{aligned} \tag{2}$$

where $\rho = |\mathbf{R}_i - \mathbf{R}_j|/R_{ij}^0$. $|\mathbf{R}_i - \mathbf{R}_j|$ is the interatomic separation distance between atoms i and j, and R_{ij}^0 and ϵ_{ij} are flexible parameters, specific to the atomic species of atoms i and j, representing the minimum energy distance and energy well depth respectively. The values of the buffering constants are set to $\delta = 0.07$ and $\gamma = 0.12$, and were originally determined from fits to noble gas data.[55] The values for R_{ii}^0/R_{jj}^0 and $\epsilon_{ii}/\epsilon_{jj}$ for homonuclear dimers were obtained from fits to MP2/aug-cc-pVTZ energies and experimental data, while values for heteronuclear dimers are calculated from the combining rules:[21]

$$R_{ij} = \frac{(R_{ii}^0)^3 + (R_{jj}^0)^3}{(R_{ii}^0)^2 + (R_{jj}^0)^2} \tag{3}$$

$$\epsilon_{ij} = \frac{4\epsilon_{ii}\epsilon_{jj}}{(\epsilon_{ii}^{1/2} + \epsilon_{jj}^{1/2})^2} \tag{4}$$

2.3 The TTM-nrg PEF

Within the TTM-nrg PEF,[23,24] water−water interactions are represented by the MB-pol PEF,[56–60] while ion−water interactions are represented by analytical functions representing ELEC, POL, DISP, and PAULI:

$$V_{\mathrm{INT}}^{\text{TTM-nrg}} = V_{\mathrm{ELEC}}^{\text{TTM-nrg}} + V_{\mathrm{POL}}^{\text{TTM-nrg}} + V_{\mathrm{PAULI}}^{\text{TTM-nrg}} + V_{\mathrm{DISP}}^{\text{TTM-nrg}} \tag{5}$$

TTM-nrg $V_{\mathrm{ELEC}}^{\text{TTM-nrg}}$ and $V_{\mathrm{POL}}^{\text{TTM-nrg}}$ terms use an extended Thole-type model[54] with exponential-4 damping to represent permanent and induced electrostatic interactions, respectively, as described in detail in refs 23 and 24. The ion dipole polarizabilities were calculated at the CCSD(T)/cc-pwCV5Z level of theory.[24]

The TTM-nrg Pauli repulsion energy, $V_{\mathrm{PAULI}}^{\text{TTM-nrg}}$, is represented by a pairwise sum of Born-Mayer functions

$$V_{\mathrm{PAULI}}^{\text{TTM-nrg}} = A_{OX}e^{-b_{OX}R_{OX}} + A_{H_1X}e^{-b_{H_1X}R_{H_1X}} + A_{H_2X}e^{-b_{H_2X}R_{H_2X}} \tag{6}$$

A_{ij} and b_{ij} in eq 6 are flexible parameters, specific to the atomic species of atoms i and j, determined by fitting to reference CCSD(T) interaction energies (after subtracting $V_{\mathrm{ELEC}}^{\text{TTM-nrg}}$ and $V_{\mathrm{POL}}^{\text{TTM-nrg}}$). The TTM-nrg dispersion energy ($V_{\mathrm{DISP}}^{\text{TTM-nrg}}$) is represented by the following function:

$$V_{\mathrm{DISP}}^{\text{TTM-nrg}} = -f_6^{TT}(\delta_{XO}R_{XO})\frac{C_{6,XO}}{R_{XO}^6} - f_6^{TT}(\delta_{XH_1}R_{XH_1})\frac{C_{6,XH_1}}{R_{XH_1}^6} - f_6^{TT}(\delta_{XH_2}R_{XH_2})\frac{C_{6,XH_2}}{R_{XH_2}^6} \tag{7}$$

$C_{6,ij}$ in eq 7, specific to atoms i and j, are fitted independently of the other terms using the exchange dipole method (XDM)[61–63] calculated with the Postg software.[64,65] Damping is achieved using the Tang-Toennies ($f_6^{TT}(\delta_{\alpha\beta})$) damping scheme.[66] Additionally, the damping parameters, δ_{ij}, are constrained to be equal to the corresponding b_{ij} parameters in eq 6.

2.4 The MB-nrg PEF

The MB-nrg PEFs for alkali ion−water interactions[19] are rigorously derived from the many-body expansion.[67] The MB-nrg PEFs adopt the same functional form and parameterizations as the TTM-nrg ELEC, POL, and DISP terms, $V_{\text{ELEC}}^{\text{TTM-nrg}}$, $V_{\text{POL}}^{\text{TTM-nrg}}$, and $V_{\text{DISP}}^{\text{TTM-nrg}}$, respectively, but replace the TTM-nrg Born-Mayer functions, $V_{\text{PAULI}}^{\text{TTM-nrg}}$, with PIPs[33] for ion−water 2B and ion−water−water 3B interactions, $V_{\text{2B}}^{\text{MB-nrg}}$ and $V_{\text{3B}}^{\text{MB-nrg}}$, respectively.

The PIPs can be thought of as quantum corrections to the underlying classical TTM-nrg-like potential, accounting for close-range PAULI and CT interactions, as well as correcting deficiencies in the TTM-nrg ELEC and DISP terms.[20] The PIPs are turned on via sigmoidal "switching functions" at small intermonomer separations, leaving the remaining TTM-nrg terms to capture long range interactions, and many-body polarization.[18,19] The PIPs are "permutationally invariant" with respect to interchangeable atoms in the system.[33] The PIPs are functions of the distances between the ion and the six sites of an MB-pol water molecule. The coefficients of both 2B and 3B PIPs were optimized using Tikhonov regression[68] (also known as ridge regression) to reproduce reference 2B and 3B energies calculated at the CCSD(T)-F12b[69,70]/CBS level of theory for Li^+−water and Na^+−water interactions, and at the CCSD(T)/CBS level of theory for K^+−water, Rb^+−water, and Cs^+−water interactions.[19]

2.5 ALMO-EDA calculations

Given a base density functional, $\mathcal{E}^{base}[\cdot]$, ALMO-EDA decomposes the interaction energy calculated with that functional, V_{INT}, into a sum of frozen, POL, and CT energies, V_{FRZ}, V_{POL}, and V_{CT}, respectively:[27]

$$V_{INT} = V_{FRZ} + V_{POL} + V_{CT} \tag{8}$$

The V_{FRZ} term can be further decomposed into a sum of ELEC, PAULI, and DISP energies, V_{ELEC}, V_{DISP}, and V_{PAULI}, respectively:[27,29]

$$V_{FRZ} = V_{ELEC} + V_{DISP} + V_{PAULI} \tag{9}$$

Since the ALMO-EDA method is discussed in detail in the original references,[26–29] we only summarize the main aspects of the method here.

The three terms on the right-hand side of eq 8 are each interaction energy components for the total system, with each term corresponding to its own total-system electron density, differing from each other in their respective degrees of relaxation (minimization of the total electronic energy). The least-relaxed (highest energy) electronic density, the frozen density, $\rho_{FRZ}(\mathbf{r})$, results from the antisymmetric product of the isolated monomer occupied orbitals (fully-relaxed in isolation, calculated with the base functional), superimposed into the complex geometry. $\rho_{FRZ}(\mathbf{r})$ is "frozen" in the sense that monomer densities are unchanged relative to their optimized, isolated densities (apart from the antisymmetrization). The frozen energy, V_{FRZ} is taken to be the difference from subtracting the sum of the isolated monomer total energies, E_{1B}^{tot}, from the total energy of $\rho_{FRZ}(\mathbf{r})$ calculated with the base functional.

$$V_{FRZ} = \mathcal{E}^{base}[\rho_{FRZ}(\mathbf{r})] - E_{1B}^{tot} = E_{FRZ}^{tot} - E_{1B}^{tot} \tag{10}$$

The decomposition of the frozen energy (eq 9) is described in detail in refs 27 and 29, but we note here that the calculation of the dispersion energy, V_{DISP}, requires the use of a "dispersion-free" XC functional, $\mathcal{E}_{DF}^{base}[\cdot]$ specific to the base functional. Ideally, $\mathcal{E}_{DF}^{base}[\cdot]$ would lack any dispersion interaction, but would otherwise be identical to the base functional. Therefore, in the interest of fair comparisons between the functionals, we only consider the sum, $V_{Pauli+Disp} = V_{PAULI} + V_{DISP}$, in the analyses presented in Section 3. We also only consider the ALMO-EDA 2 "classical" ELEC energy[27,29] in order to make meaningful comparisons between the decompositions of XC functionals with those obtained with the

PEFs. We also make use of the kinetic energy pressure (KEP) in section 3.4

The POL energy, V_{POL}, is calculated from the total-system electron density obtained via relaxation with respect to the base functional, such that each monomer polarizes each other monomer, but no electron density is transferred between the monomers. This is accomplished by only allowing monomer electron densities to relax within their own "polarization subspaces. In ALMO-EDA 2, these subspaces are determined with the use of fragment electric field response functions.[27,28,30] V_{POL} is then computed by subtracting E_{1B}^{tot} and V_{FRZ} from the total energy of the polarized density, $\rho_{POL}(\mathbf{r})$ calculated with the base functional:

$$V_{POL} = \mathcal{E}^{base}[\rho_{POL}(\mathbf{r})] - E_{1B}^{tot} - V_{FRZ} \tag{11}$$

The CT energy, V_{CT}, is calculated from the fully-relaxed total-system electron density, $\rho_{SCF}(\mathbf{r})$, (i.e. what one would obtain from an unconstrained DFT calculation with the base functional). This electron density can be thought of as resulting from mixing each monomer's (polarized) occupied orbitals from $\rho_{POL}(\mathbf{r})$ with the occupied and virtual orbitals of the surrounding monomers (as well as its own virtual orbitals).[27,28,30] The total interaction energy, V_{INT}, is calculated by subtracting E_{1B}^{tot} from the total energy of $\rho_{SCF}(\mathbf{r})$ with respect to the base functional. The CT energy, V_{CT}, is finally calculated by subtracting V_{FRZ} and V_{POL} from V_{INT},

$$V_{INT} = \min_{\rho_{SCF}(\mathbf{r})} \mathcal{E}^{base}[\rho_{SCF}(\mathbf{r})] - E_{1B} = E_{SCF}^{tot} - E_{1B}^{tot} \tag{12}$$

$$V_{CT} = V_{INT} - V_{FRZ} - V_{POL} \tag{13}$$

The ALMO-EDA 2 method[27] was used in all energy decompositions that were carried out using the following XC functionals: BLYP,[71,72] PBE,[73] revPBE,[74] SCAN,[75] TPSS,[76] B97M-rV,[77,78] B3LYP,[79] PBE0,[80] revPBE0, M06-2X,[81] ωB97X,[82] and ωB97M-V.[77,83] Excluding B97M-rV and ωB97M-V, all DFT energies were calculated with and without the

D3(0) empirical dispersion corrections.[84] Since ωB97X-D uses D2 empirical dispersion corrections[85] which are unavailable for Cs, we do not include ωB97X-D in our analysis, but do briefly discuss its accuracy in 2B energies of $K^+(H_2O)$ and $Rb^+(H_2O)$ dimers in section 3.2. It should also be noted that in addition to using D2 corrections, the ωB97X-D functional itself has a different parameterization than that of ωB97X, which means that ALMO-EDA terms other than the DISP energy will differ between the ωB97X-D and ωB97X-D3. All ALMO-EDA 2 calculations were carried out with Q-Chem 5.1[86] and used the same basis sets as those used in the reference CCSD(T) calculations (section 2.1).

3 Results

3.1 Many-Body Halide–Water Models

To assess the ability of AMOEBA, TTM-nrg, and MB-nrg to describe alkali ion−water interactions, Figure 2 shows comparisons with CCSD(T) interaction energies calculated for radial scans obtained by moving each alkali ion along the direction of the water H−O−H bisector, as described in section 2.1. The most apparent feature seen here is the tendency of the AMOEBA to produce interaction energies that are too repulsive at close range for all dimers except for $K^+(H_2O)$, for which AMOEBA is slightly too repulsive near the minimum-energy distance (by less than 0.5 kcal/mol), and becomes slightly too attractive at close range (by around −2 kcal/mol at an K^+−O distance of 2 Å. For all other dimers, but most significantly for $Rb^+(H_2O)$ and $Cs^+(H_2O)$, the AMOEBA interaction energy converges to the reference CCSD(T) interaction energy at long range where the permanent electrostatics are the dominant interaction,[14] but becomes too repulsive at too large of an M^+−O distance. This artificially-steep repulsive wall results in overestimation of the minimum-energy distances by around 0.2 Å in both $Rb^+(H_2O)$ and $Cs^+(H_2O)$. The AMOEBA 2B energy was also found to diverge from CCSD(T)-F12b at close range in halide−water dimers scanned along the water O−H axis, producing 2B curves that were too repulsive (and too steep) at too large an

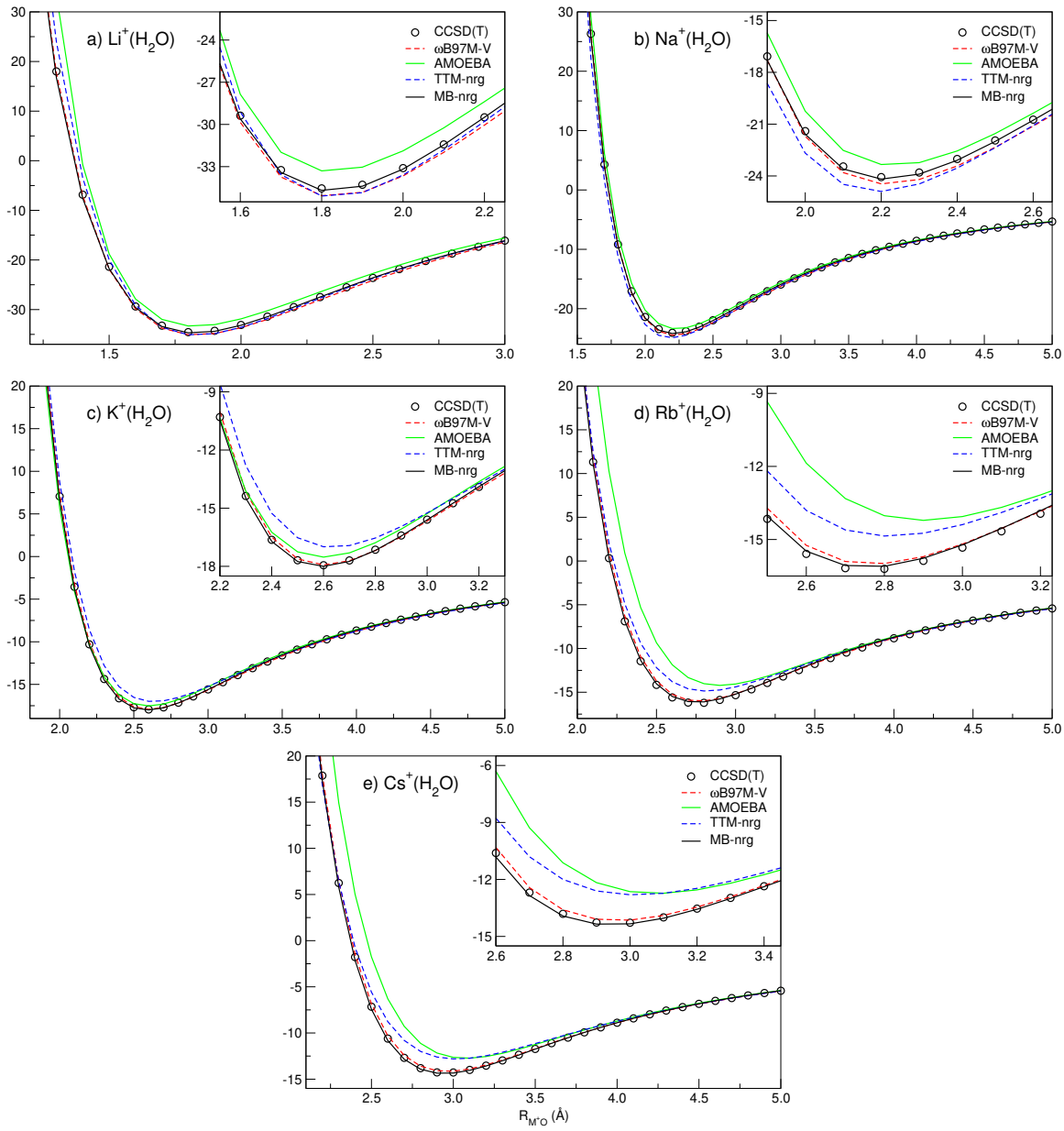

Figure 2: Comparisons between CCSD(T) (open circles) and ωB97M-V (dotted red), AMOEBA (solid green), TTM-nrg (dotted blue), and MB-nrg (solid black) interaction energies calculated for radial scans of $M^+(H_2O)$ dimers, with M = Li (a), Na (b), K (c), Rb (d), Cs (e), in which each alkali ion in displaced along the water H−O−H bisector, on the opposite side of the water-hydrogens, in the water-plane, as described in section 2.1.

X^-−O distance, leading to overestimated minimum-energy distances.[20] However, AMOEBA additionally predicts minimum energies that are too attractive in the halide−water dimer scans,[20] while we find here that AMOEBA predicts minimum energies that are too repulsive

in the alkali−water scans.

TTM-nrg performs better than AMOEBA on average in all dimer scans except for parts of the $Na^+(H_2O)$ and $K^+(H_2O)$ scans. It should be noted, however, that despite performing better than AMOEBA on average, TTM-nrg deviates from the CCSD(T) reference energies by around 2 kcal/mol or more in some configurations at close range in each dimer scan. As is the case for AMOEBA, TTM-nrg appears to converge to the CCSD(T) curves at long range. This agreement of AMOEBA and TTM-nrg with CCSD(T) at long range is consistent with the fact that both models use similar representations of the ELEC energy, which is the dominant interaction at large ion−water separations.[14] While TTM-nrg tends to find the correct minimum-energy distances along each scan, the TTM-nrg 2B interaction energies at the minima differ from the corresponding CCSD(T) values by more than 1 kcal/mol in $K^+(H_2O)$, $Rb^+(H_2O)$ and $Cs^+(H_2O)$. Interestingly, this behavior was not apparent in the the halide−water TTM-nrg scans, which were slightly too repulsive in the close range repulsive region, but were otherwise quite accurate at all other ion−water separations except for $F^-(H_2O)$, in which TTM-nrg predicted that the minimum energy was around 1.3 kcal/mol lower than the CCSD(T) value.[20]

MB-nrg remains within 1 kcal/mol of the CCSD(T) 2B energies along each scan. The largest deviations of MB-nrg relative to CCSD(T) occur within the repulsive regions in each scan, but the deviations remain within roughly 0.25 kcal/mol at medium and long ranges. Given that the MB-nrg differs from TTM-nrg only by the replacement of the TTM-nrg Born-Mayer repulsive potential with PIPs (Section 2.4), the higher accuracy of MB-nrg than TTM-nrg at all configurations along each scan demonstrates the importance of including effective quantum corrections to the TTM-nrg classical interactions at close range, keeping in mind that TTM-nrg reproduces the CCSD(T) 2B energies in the long range regime of each scan.

3.2 2B Interaction Energies

Figure 3 shows the deviations of the total 2B interaction energies calculated with each tested model relative to CCSD(T)/CBS for each of the five $M^+(H_2O)$ dimers in their corresponding minimum-energy geometries obtained from MP2 optimizations (section 2.1). For reference, a dashed line, indicating the ±1 kcal/mol threshold that is generally used to define "chemical accuracy," is also shown in each panel of Figure 3. Similar comparisons for other alkali ion−water dimer geometries are reported in the Supporting Information.

Some general trends are apparent when comparing the performance of a given method across different $M^+(H_2O)$ dimers. Notably, all non-dispersion-corrected functionals except for ωB97X produce 2B energies that tend to become less attractive and/or more repulsive than CCSD(T) with increasing ion size from $Li^+(H_2O)$ to $Rb^+(H_2O)$, while ωB97X 2B errors become less positive and more negative with increasing ion size for all dimers. Following this trend, functionals such as B3LYP and PBE0 have negative errors for $Li^+(H_2O)$, but positive errors for $Cs^+(H_2O)$. Since many of the functionals have positive errors for the dimers of the larger ions, the inclusion of D3 corrections appears to substantially improve the 2B energies (notably in B3LYP-D3), although functionals such as BLYP-D3, revPBE-D3, TPSS-D3, and revPBE0-D3 still show errors around 1 kcal/mol. ωB97X has large negative errors for these dimers, so the D3 corrections significantly worsen the 2B energies. ωB97X-D (which, for the reasons mentioned in section 2.5, is not shown in Figure 3) produces more accurate 2B energies in $K^+(H_2O)$ (−17.4 kcal/mol), and in $Rb^+(H_2O)$ (−15.7 kcal/mol) than ωB97X-D3, although these energies differ from the CCSD(T) values by more than 0.5 kcal/mol each.

It is also apparent that most models show similar accuracy for $Rb^+(H_2O)$ and $Cs^+(H_2O)$, with the largest differences in accuracy between the dimers of the two largest ions occurring in AMOEBA (−0.58 kcal/mol), ωB97X-D3 (−0.38 kcal/mol), ωB97X (−0.27 kcal/mol), revPBE-D3 (−0.17 kcal/mol), B3LYP (0.16 kcal/mol), and TTM-nrg (0.15 kcal/mol). It is interesting that most models have 2B interaction energy errors within 0.1 kcal/mol between $Rb^+(H_2O)$ and $Cs^+(H_2O)$, despite the fact that the reference CCSD(T) 2B energies for the

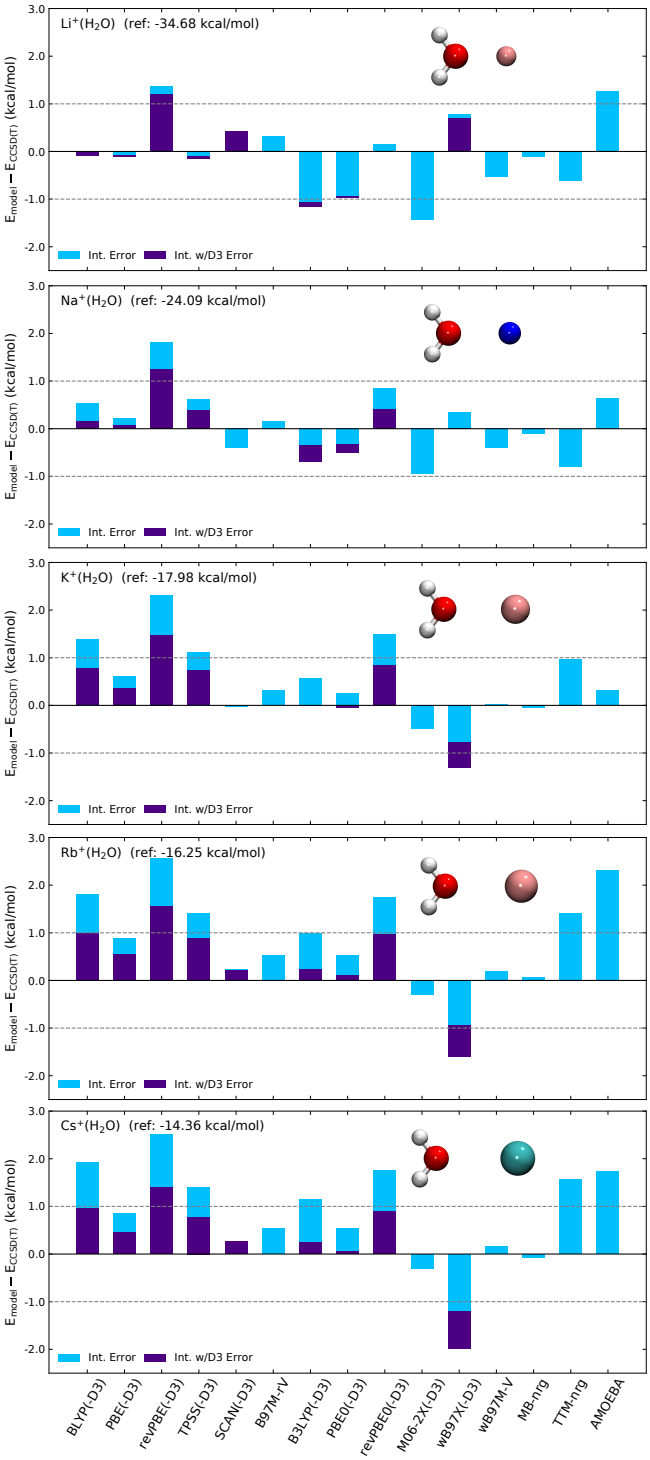

Figure 3: Deviations from the CCSD(T) 2B interaction energies of the $M^+(H_2O)$ dimers with M = Li (a), Na (b), K (c), Rb (d), Cs (e), in the corresponding minimum energy configurations (from MP2 as described in section 2.1) calculated with various XC functionals as well as the AMOEBA, TTM-nrg, and MB-nrg PEFs.

two dimers differ by around 2 kcal/mol.

Among the GGA functionals considered in this study, revPBE without D3 corrections significantly underestimates the interaction strength in all dimers, deviating from the CCSD(T) 2B energies by more than 1 kcal/mol for each. BLYP also underestimates the interaction strength of all dimers other than $Li^+(H_2O)$, for which it deviates from CCSD(T) by 0.01 kcal/mol. BLYP has errors greater than 1 kcal/mol for $K^+(H_2O)$, and errors just under 2 kcal/mol in $Rb^+(H_2O)$, and $Cs^+(H_2O)$, but is still more accurate than revPBE for all alkali ion−water dimers. Furthermore, revPBE appears to have the largest errors on average among all functionals, deviating from CCSD(T) by over 1 kcal/mol in $Li^+(H_2O)$ (for which M06-2X has similar accuracy), and deviating by around 2.5 kcal/mol in $Rb^+(H_2O)$ and $Cs^+(H_2O)$. PBE performs the best out of the GGA functionals, having errors just below 1 kcal/mol in $Rb^+(H_2O)$ and $Cs^+(H_2O)$, and errors below 0.25 kcal/mol in $Li^+(H_2O)$ and $Na^+(H_2O)$.

Among the meta-GGA functionals considered here, SCAN and B97M-rV perform the best, both deviating from CCSD(T) by at most 0.5 kcal/mol for all dimers. TPSS yields 2B energies that are too repulsive for all dimers other than $Li^+(H_2O)$, for which it has a small negative error, leading to significant improvements upon adding the D3 corrections. Interestingly, the accuracy of TPSS-D3 is comparable to that of BLYP-D3 for all minimum energy dimers.

The hybrid functionals have varied performance, with ωB97M-V being, on average, the most reliable hybrid functional for all dimers, revPBE0 and ωB97X-D3 being the least accurate hybrid functionals for dimers of the larger ions, and with M06-2X being the least accurate hybrid functional for $Li^+(H_2O)$ and $Na^+(H_2O)$. PBE0 tends to benefit from D3 corrections, such that PBE0-D3 deviates from CCSD(T) by around 0.1 kcal/mol for all dimers except for $Li^+(H_2O)$ and $Na^+(H_2O)$, for which it has errors of around -1 and -0.5 kcal/mol, respectively. B3LYP benefits from D3 corrections as well, having errors within 0.25 kcal/mol for all dimers except for $Li^+(H_2O)$ and $Na^+(H_2O)$, for which its errors are

comparable to those for PBE0.

AMOEBA underestimates the strength of the interactions in all alkali ion−water dimers, deviating from the CCSD(T) 2B energies by at most 2.3 kcal/mol in $Rb^+(H_2O)$, and by as little as 0.3 kcal/mol in $K^+(H_2O)$. AMOEBA is among the least accurate models in $Li^+(H_2O)$, $Rb^+(H_2O)$, and $Cs^+(H_2O)$, although it outperforms revPBE in all dimers. TTM-nrg also underestimates the interaction strength in $Rb^+(H_2O)$, and $Cs^+(H_2O)$, having errors of 1.4 and 1.6 kcal/mol, respectively. TTM-nrg and AMOEBA exhibits similar accuracy for $Cs^+(H_2O)$ and $Na^+(H_2O)$, but AMOEBA is more accurate than TTM-nrg for $K^+(H_2O)$. Interestingly, TTM-nrg shows negative errors in $Li^+(H_2O)$ and $Na^+(H_2O)$, but positive errors for all other dimers. MB-nrg is, on average, the most accurate model for all alkali ion−water dimers, deviating from CCSD(T) by at most −0.1 kcal/mol in both $Li^+(H_2O)$ and $Na^+(H_2O)$.

3.3 3B Interaction Energies

Figure 4 shows the deviations of the 3B energy calculated with each model relative to CCSD(T)/CBS for each of the five minimum-energy alkali ion−water $M^+(H_2O)_2$ trimers. The deviations of each model relative to CCSD(T)/CBS for all stable alkali ion−water $M^+(H_2O)_2$ trimers are reported in the Supporting Information. Dotted lines on each plot indicate the ±1 kcal/mol "chemical accuracy" threshold. Similar comparisons for the other alkali ion−water trimer geometries are reported in the Supporting Information.

All XC functionals have deviations within 1 kcal/mol for each trimer. $Li^+(H_2O)_2$ has the largest mean absolute 3B errors among the XC functionals (0.29 kcal/mol), while $Rb^+(H_2O)_2$ has the lowest mean absolute error (0.09 kcal/mol). It should be noted that $Li^+(H_2O)_2$ also has the largest reference 3B energy of 3.37 kcal/mol, which is a factor of two larger than that of $Na^+(H_2O)_2$. The second largest 3B energy. In the analysis of halide−water trimers, it was found that the 3B errors were very uniform between the different systems, such that the $F^-(H_2O)_2$ and $Cl^-(H_2O)_2$ minimum energy isomers have the largest and smallest mean absolute errors of 0.27 and 0.23 kcal/mol, respectively.

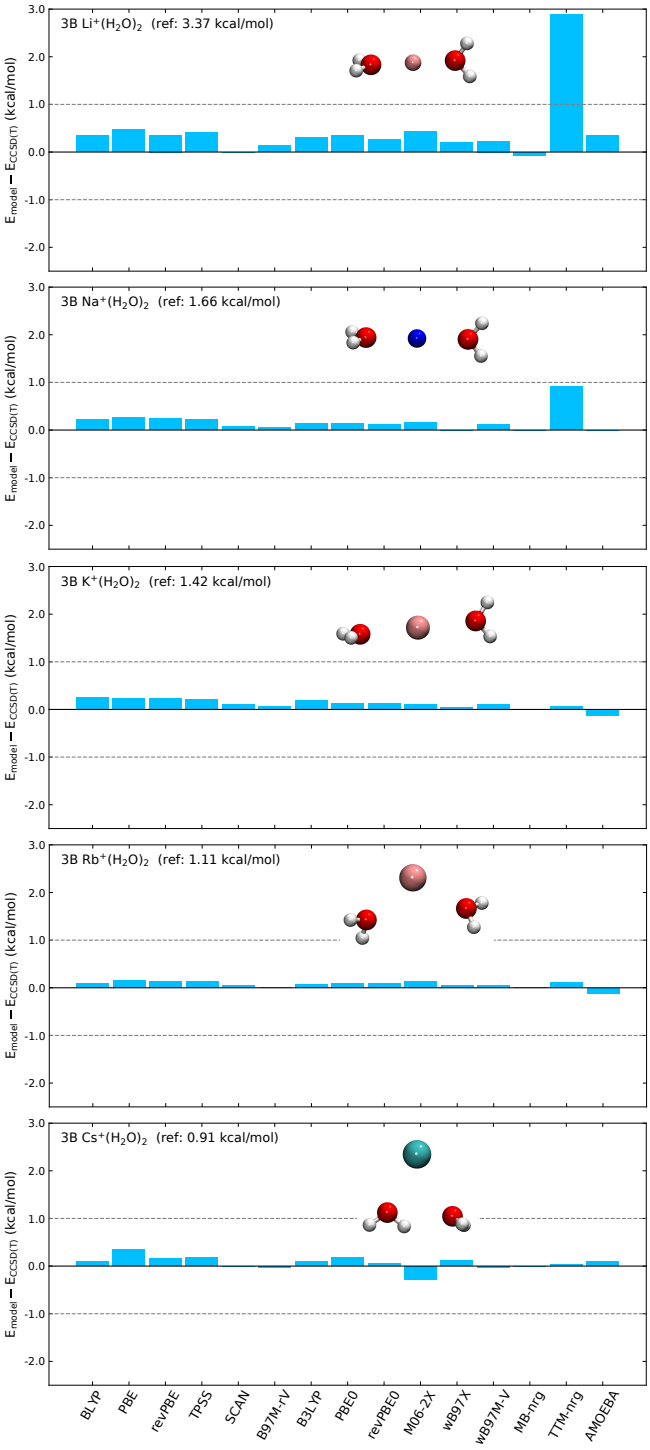

Figure 4: Deviations from the CCSD(T) 2B interaction energies of the $M^+(H_2O)_2$ trimers with M = Li (a), Na (b), K (c), Rb (d), Cs (e), in the corresponding minimum energy configurations (from MP2 as described in section 2.1) calculated with various XC functionals as well as the AMOEBA, TTM-nrg, and MB-nrg PEFs.

Nearly all functionals predict 3B energies that are more repulsive than the CCSD(T) reference value for all trimers, with the exception being M06-2X for $Cs^+(H_2O)_2$. All other negative errors have magnitudes less than 0.05 kcal/mol. It was also found that most of the tested XC functionals predict halide−water 3B energies that are more repulsive than the CCSD(T)-F12b reference values for the minimum energy halide−water $X^-(H_2O)_2$ trimers, such that all negative errors have magnitudes less than 0.05 kcal/mol.[20]

Among the XC functionals, SCAN, B97M-rV, and ωB97X yield the best 3B energies, averaged over the minimum-energy geometries, each deviating from the CCSD(T) reference 3B values, on average, by no more than 0.1 kcal/mol. PBE has the largest mean absolute error among the functionals (0.30 kcal/mol). For the minimum energy halide−water trimers, revPBE0, ωB97X-D, and ωB97M-V produced the most accurate 3B energies, while PBE produced the least accurate 3B energies.[20]

Among the PEFs, TTM-nrg shows very large, positive 3B energy errors for the $Li^+(H_2O)_2$ and $Na^+(H_2O)_2$ trimers in their minimum-energy geometries, deviating from the CCSD(T) reference by 2.88 and 0.92 kcal/mol, respectively. Given that the TTM-nrg ion−water−water 3B energy is entirely due to classical POL, these large errors may suggest that close-range quantum effects such as CT may be important for reproducing these 3B interactions. However, the AMOEBA PEFs yields 3B energies for $Li^+(H_2O)_2$ and $Na^+(H_2O)_2$ that deviate from the CCSD(T) 3B energy by −0.34 and 0.01 kcal/mol, respectively, despite being composed solely of classical POL, themselves. Looking at the energy decomposition analysis of 2B interaction energies of $Li^+(H_2O)$ and $Na^+(H_2O)$ dimers, as well as decompositions of 3B energies of $Li^+(H_2O)_2$ and $Na^+(H_2O)_2$ trimers, it appears that AMOEBA tends to produce POL energies that are similar to ALMO-EDA POL energies of XC functionals, while TTM-nrg and MB-nrg (classical) POL energies tend to be larger in magnitude than the corresponding ALMO-EDA values. Note that there is widespread agreement between the tested XC functionals with respect to their ALMO-EDA POL energies. This difference in POL energies between AMOEBA and TTM-nrg for Li^+ and Na^+ dimers and trimers could

be due to a combination of factors, including differences in atom-centered dipole polarizabilities, differences in permanent charges, the use of permanent dipoles and quadrupoles in AMOEBA, differences in Thole damping parameters, or in the different damping schemes used by each model (see section 2). These differences in POL energies between the two sets of models may be accentuated in the Li^+ and Na^+ dimers and trimers due to the small distances between the ion and the water molecule(s) in these structures, compared to those in the K^+, Rb^+, and Cs^+ dimers and trimers. We note, however, that TTM-nrg was found to predict, on average, better 3B energies for halide−water trimers than AMOEBA,[20] indicating some amount of error cancellation, for example in the non-negligible 3B CT energies found in alkali ion−water trimers (see the Supporting Information), and in halide−water trimers (see the Supporting Information of reference 20).

Irrespective of the underlying cause leading to the large deviations in the TTM-nrg 3B interaction energies of the minimum energy $Li^+(H_2O)_2$ and $Na^+(H_2O)_2$ trimers, Figure 4 demonstrates that the 3B MB-nrg PIPs (section 2.4) provide sufficiently accurate close-range corrections to the underlying classical model, which for 3B and higher-body energy terms, is identical to those of TTM-nrg.

3.4 Energy Decomposition Analysis

Decompositions of the 2B energies of the $M^+(H_2O)$ dimers are reported in Figure 5. Statistics for 2B ALMO-EDA calculations of alkali ion−water $M^+(H_2O)$ dimers and $M^+(H_2O)_2$ trimers are reported in the Supporting Information to aid in the analysis. Additionally, statistics for 2B ALMO-EDA calculations of halide−water $X^-(H_2O)$ dimers taken from ref 20 are also reported in the Supporting Information for comparison with the alkali ion water dimer statistics. Interestingly, some of the trends found in the analysis of energy decompositions of 2B energies of halide−water dimers[20] are not reproduced in the analogous decompositions of the 2B energies of the alkali ion−water dimers. Differences in trends between the halide−water and alkali ion−water decompositions could be due to differences in the descriptions of the ion,

in particular because anionic species are more difficult to describe with semi-local functionals than neutral or cationic species.[87] Differences between halide−water and alkali ion−water decompositions could also be due to differences in the variations among the functionals in their descriptions of the water hydrogens and the water oxygen, since halide ions accept hydrogen bonds from the water molecule while alkali ions are bound to the water oxygen.

One notable difference between halide−water and alkali ion−water energy decompositions is that the $Li^+(H_2O)$ ELEC energy has a larger standard deviation (0.7 kcal/mol) than any other interaction term among XC functionals, while the ELEC energy is very consistent among all XC functionals in all halide−water dimers, with $F^-(H_2O)$ having the largest standard deviation of 0.3 kcal/mol (relative to all functionals from all classes of XC functionals).[20] The mean ELEC energies (and their standard deviations) in $Li^+(H_2O)$ for GGA, meta-GGA, and hybrid functionals are found to be −31.4 (0.2), −32.0 (0.4), and −32.8 (0.3) kcal/mol, respectively. Relative uniformity within XC functional classes, but large deviations between the classes, suggests that nonlocal effects due to the use of the kinetic energy density in meta-GGAs and more significantly, Hartree-Fock exchange in hybrid functionals, might be necessary for describing the ELEC energy in $Li^+(H_2O)$. It should be noted, however, that the GGA functionals BLYP and PBE yield more accurate total 2B energies of the $Li^+(H_2O)$ dimer, relative to the CCSD(T) reference, than a number of hybrid functionals, such as M06-2X, B3LYP, PBE0, and ωB97X, which indicates that the accurate reproduction of the $Li^+(H_2O)$ ELEC term is more complicated than simply adding Hartree-Fock exchange.

It is likely that the large deviation of the $Li^+(H_2O)$ ELEC energy trend from the trends seen in halide−water dimers is at least in part due to the fact that Li^+ has no isoelectronic counterpart in the halide ions. However, we point out that Figure 5 (and Tables S1 and S2 in the Supporting Information) shows that ELEC energies of the other alkali ion−water dimers have, on average, more variance than the halide−water ELEC energies.[20] Figure 5 shows that ELEC energies calculated with GGA and meta-GGA functionals in the other alkali−water dimers tend to be very similar, with the two classes having mean values within

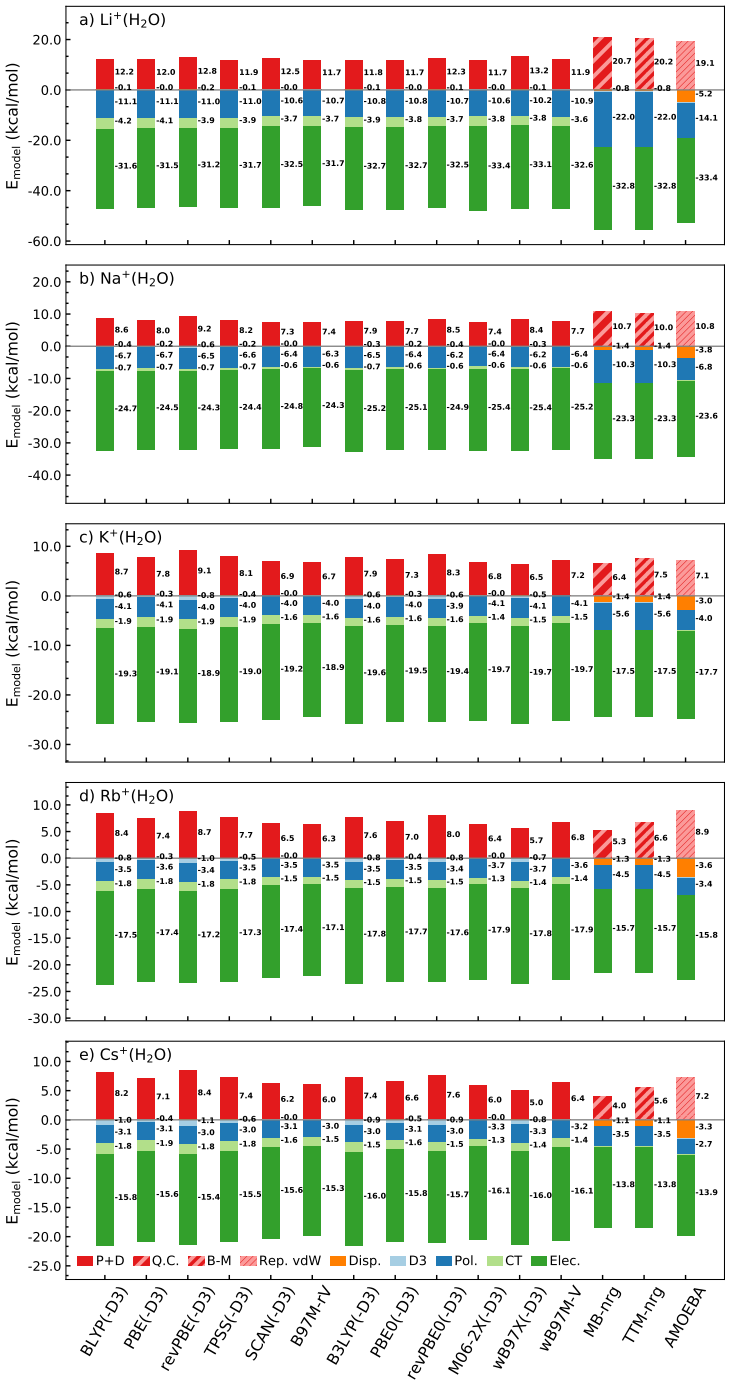

Figure 5: Energy decompositions for each minimum energy $M^+(H_2O)$, with M = Li (a), Na (b), K (c), Rb (d), Cs (e), with numerical energy values (in kcal/mol) shown on the right-hand side of each bar.

0.1 kcal/mol of each other.

However, the ELEC energies of all alkali ion−water dimers calculated with the hybrid

functionals are, on average, more attractive than those calculated with the semi-local functionals, although differences between the values calculated with hybrid functionals and semi-local functionals become smaller with increasing ion size. Since the ELEC energy is calculated within the ALMO-EDA frozen energy term, differences between functionals reflect differences in their descriptions of the electronic structures of the isolated monomers. The fact that all dimers other than $Li^+(H_2O)$ have relatively uniform ELEC energies among the functionals suggests that the large variance in $Li^+(H_2O)$ is likely due to differences in descriptions of Li^+ between the functionals given that the water molecules are similarly distorted between the dimers. However, it is also possible that the small distance between Li^+ and the water oxygen (around 1.8 Å) accentuates differences in the electronic structures of the isolated water produced by each functional compared to those in the other dimers.

The Pauli+Disp terms are the most varied among all functionals for all alkali ion−water dimers except for $Li^+(H_2O)$. The variance in Pauli+Disp energies increases with increasing ion size, with the standard deviations (among all functionals) for $Li^+(H_2O)$ and $Cs^+(H_2O)$ being 0.5 and 1.0 kcal/mol, respectively. Pauli+Disp is also the most varied interaction term for all halide−water dimers, although it was found that the standard deviation decreases with increasing ion size, with the standard deviations for $F^-(H_2O)$ and $I^-(H_2O)$ being 2.2 and 1.0 kcal/mol, respectively.[20] The difference in this variance trend likely reflects the fact that Pauli+Disp energies represent increasing (negative) fractions of the total 2B interaction energy of alkali ion−water dimers with increasing ion size, while representing decreasing (negative) fractions of the total 2B energy of halide−water dimers with increasing ion size.[20]

One notable similarity between energy decompositions of the alkali ion−water dimers and the halide−water dimers is that Pauli+Disp energies predicted by hybrid functionals are, on average, less repulsive than those predicted by GGA functionals.[20] One possible explanation of this trend stems from the inability of GGA functionals to reproduce intermediate to long range (attractive) dispersion interactions, which requires a nonlocal treatment of electron correlation.[88–91] The fact that the meta-GGA functionals tested here predict

Pauli+Disp energies that are comparable to (and sometimes even less repulsive than) those predicted by hybrid functionals supports this hypothesis, since the use of the kinetic energy density adds more nonlocal character to the correlation energy of an XC functional. In particular, the meta-GGA SCAN functional has been shown to capture intermediate-range dispersion,[75,89] and the meta-GGA B97M-rV includes the explicitly nonlocal rVV10 correlation functional.[90] We point out that hybrid GGA XC functionals have been shown to lack dispersion interactions,[89,91] which appears to be consistent with the fact that B3LYP and revPBE0 tend to yield Pauli+Disp energies that are more repulsive than those from hybrid meta-GGAs (M06-2X, ωB97X, and ωB97M-V), SCAN, and B97M-rV, especially in the dimers of the larger ions. The hybrid GGA PBE0 appears to be an exception to this finding, likely benefiting from error cancellation, resulting from the fact that PBE yields less repulsive Pauli+Disp energies than BLYP and revPBE due to the behavior of its exchange energy with respect to the electronic density gradient.[20] Note that these trends in the Pauli+Disp energies for GGAs, meta-GGAs, hybrid GGAs, hybrid meta-GGAs, can also be seen in the halide−water dimer EDA in reference 20.

A second possible explanation for the trend in the differences between GGA and hybrid Pauli+Disp energies is based on the tendency of semi-local functionals to artificially delocalize electron density while Hartree-Fock exchange localizes the electron density.[37,38] Excessive delocalization of the isolated monomer electron densities may result in spurious Pauli repulsion in the frozen-electronic state (section 2.5) of dimers at small intermonomer separations, which would lead to the observed trends. Furthermore, the fact that differences between GGA and hybrid Pauli+Disp energies are more pronounced in the halide−water dimers[20] strengthens this argument since anionic species tend to suffer from artificial delocalization more than neutral or cationic species.[87] The dominant repulsive interaction contributing to the ALMO-EDA Pauli repulsion energy is the kinetic energy pressure (KEP), which can be thought of as the (primarily kinetic) energetic penalty paid to orthogonalize isolated monomer electron wavefunctions when brought into the complex geometry in the

ALMO-EDA frozen state, and therefore quantifies the importance of the second explanation. Although the ALMO-EDA KEP is inaccessible in calculations with ECPs, Tables S1 and S2 (in the Supporting Information) provide strong evidence that artificial delocalization contributes significantly to the observed differences between Pauli+Disp energies calculated with GGAs compared to hybrid functionals. It should be noted, however, that the analysis presented in ref 38 indicates that non-hybrid meta-GGA functionals suffer from delocalization errors comparable to those seen in GGA functionals. This suggests that the trends in Pauli+Disp energies produced by the semilocal meta-GGA functionals (in both alkali ion−water and halide−water dimers) would not be explained by the delocalization error, which would mean that intermediate-range dispersion interactions also play a role in the observed trends. Finally, we point out that these trends exist in all dimers, despite the accuracy of the GGAs degrading with increasing alkali ion size (section 3.2), indicating that the inclusion of nonlocal terms is necessary for an XC functional to be able to correctly reproduce Pauli+Disp energies in alkali ion−water dimers.

As a direct consequence of the delocalization error in DFT, it was found that CT energies in halide−water dimers calculated with GGA functionals are more attractive than those calculated with meta-GGA functionals, which are more attractive than those calculated with hybrid functionals.[20] The same trends seen in halide−water dimer CT energies can also be seen in the alkali−water dimers, but to a smaller extent. For example, while the difference in mean CT energies calculated with GGA and hybrid functionals was found to be 2.4 kcal/mol in $F^-(H_2O)$, the largest difference in mean CT energies between the GGAs and the hybrid functionals in the alkali−water dimers is 0.4 kcal/mol in $Cs^+(H_2O)$. This is likely due to differences in electron diffusivity in the anionic halide ions compared to the partial negative charge on the water oxygen, the primary electron donors in the halide−water and alkali ion−water dimers, respectively.

Polarization appears to be the contribution that behaves most consistently between the halide−water dimers and alkali ion−water dimers, having the smallest deviation among XC

functionals for all ions. The variance in the POL energy among functionals decreases with increasing alkali ion size, likely reflecting the trend in variance of the ELEC energy. The variance in the POL energies was also found to decrease with increasing halide ion size in the halide−water dimers.[20]

It was found that there is a correlation between the total 2B interaction energies and total 2B ALMO-EDA frozen energies of halide−water dimers predicted by various XC functionals.[20] It was suggested that this correlation might be due to the similarity in the definitions of these two energies (see eqs 12 and 10).[20] As shown in Figure 6, we find a similar correlation in alkali ion−water dimers as well. Two best-fit lines are shown for each dimer, one is fitted to all functionals from all classes, and the other is fitted to the hybrid functionals. Based on each of these best-fit lines, estimates for the total frozen energies (the y-intercepts of each line, where the interaction energy error is 0.0) are also shown in horizontal dotted lines. As was the case for halide−water dimers, the correlation apparently improves with increasing ion size. Additionally, the two sets of best-fit lines tend to converge for alkali ion−water and halide−water dimers with increasing ion size.

Figure 5 also shows energy decompositions calculated with the three PEFs studied here. As was mentioned in section 3.3, we find here that the AMOEBA 2B POL energies are relatively similar to those calculated with ALMO-EDA, whereas TTM-nrg and MB-nrg 2B POL energies tend to be larger in magnitude (i.e. more attractive) than the corresponding ALMO-EDA 2B POL values, particularly for $Li^+(H_2O)$ and $Na^+(H_2O)$. It can be seen, however, that the TTM-nrg and MB-nrg 2B POL energy agrees with the ALMO-EDA 2B POL energies for $Cs^+(H_2O)$, while the AMOEBA 2B POL energy is smaller in magnitude (less attractive) than those from ALMO-EDA. This finding that the TTM-nrg 2B POL energies are consistently more attractive than the AMOEBA 2B POL energies across the alkali ion−water dimers agrees with the plots of the 2B POL energies scanned along the water−oxygen−ion distance (as described in section 2.1) in panels b, d, and f of Figure 7 which show that the AMOEBA 2B POL energy is more damped than the TTM-nrg 2B POL

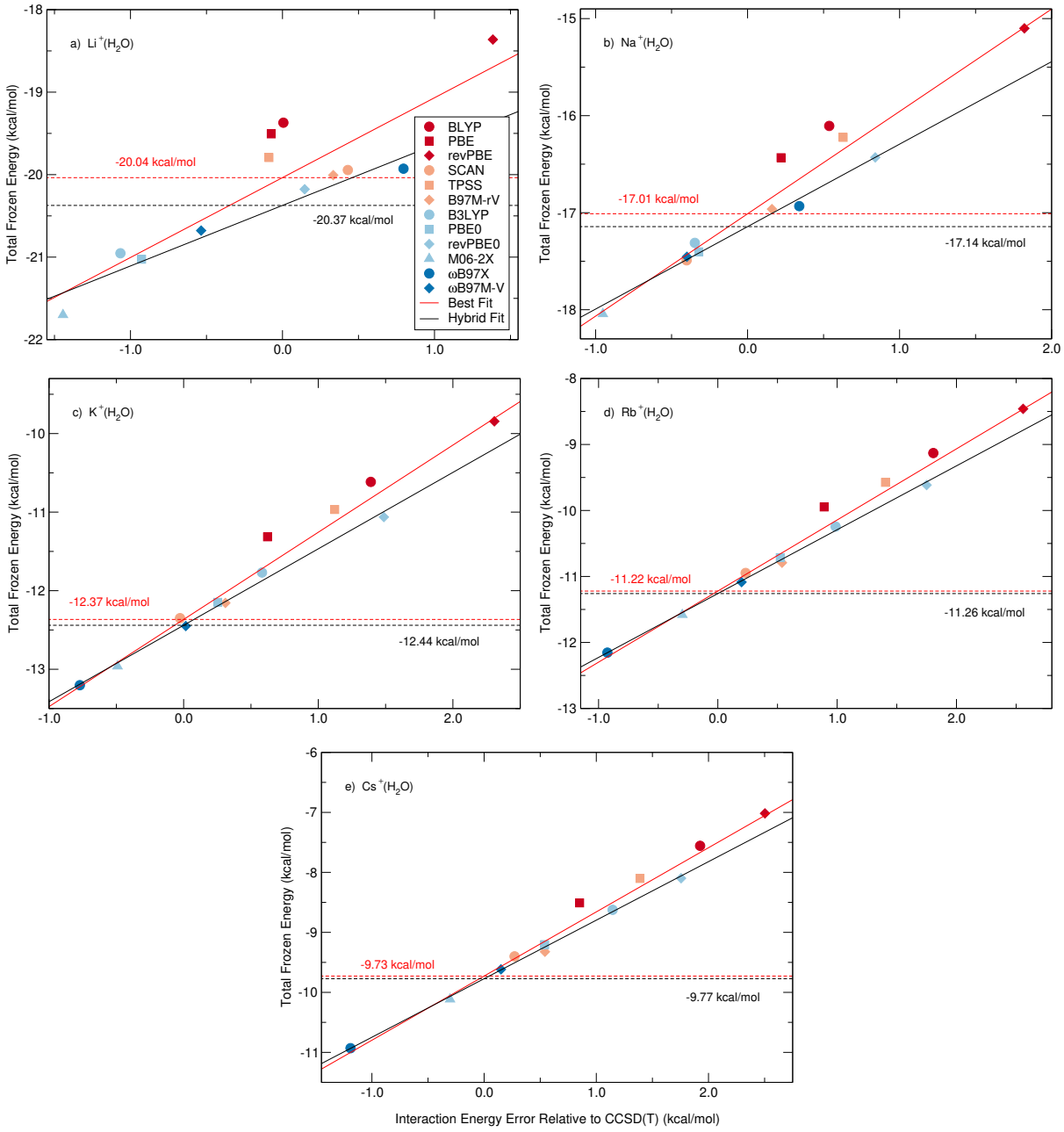

Figure 6: Total frozen energy from ALMO-EDA plotted against interaction energy deviations (relative to CCSD(T)) for $M^+(H_2O)$ dimers with M = Li (a), Na (b), K (c), Rb (d), Cs (e), for each XC functional, demonstrating the correlation between the two quantities. The best fit lines with respect to all functionals are shown as red solid lines, and the best fit lines with respect to all hybrid functionals are shown as black solid lines. The y-intercepts for each best fit line are also shown, giving an estimate of the "most accurate" total frozen energies for each dimer.

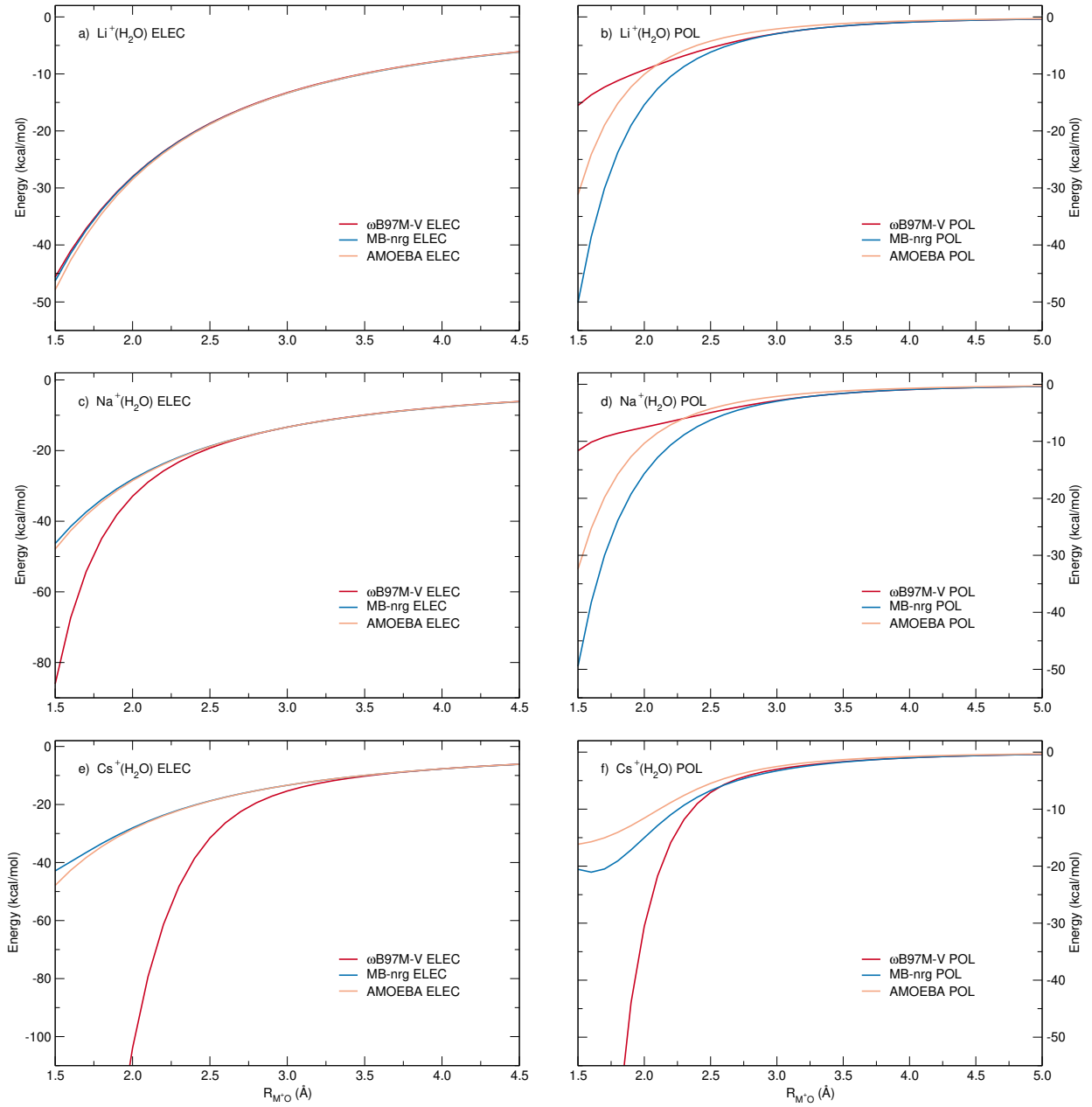

Figure 7: ELEC and POL energies calculated with each of the three sets of PEFs analyzed in this study, and the ωB97M-V functional (from ALMO-EDA) along the scans described in section 2.1 for the $Li^+(H_2O)$ (panels a and b), $Na^+(H_2O)$ (panels c and d), and $Cs^+(H_2O)$ (panels e and f) dimers.

energy.

Figure 5 shows that the ELEC energies of the minimum energy alkali−water dimers calculated with each of the tested PEFs are similar to those calculated with ALMO-EDA.

This is in contrast with the ELEC energies of halide−water dimers calculated with the PEFs, which were consistently less attractive than those calculated with ALMO-EDA. Panels a, c, and e of Figure 7 shows that the PEF ELEC energies converge to the ALMO-EDA (ωB97M-V) ELEC energies at long range, but remain less attractive than the ALMO-EDA ELEC energies as the water−oxygen−ion distance decreases. This divergence between the two sets of ELEC energies is due to the lack of attractive charge penetration interactions in the PEFs, which employ (damped) partial atomic charges. The fact that PEF ELEC energies agree with ALMO-EDA ELEC energies in the minimum energy alkali ion−water dimers indicates that these structures have oxygen−ion distances that lie outside the onset of charge penetration effects. Additionally, it should be noted that a divergence in the ELEC energies are not seen in the $Li^+(H_2O)$ scans because charge penetration effects occur at smaller Li^+−oxygen distances due to the small radius of Li^+.

The only difference between decompositions of the TTM-nrg and MB-nrg 2B interaction energies is in their Pauli+Disp terms, for which TTM-nrg uses pairwise Born-Mayer functions, while MB-nrg uses the 2B PIPs (section 2). As seen in Figure 5, MB-nrg Pauli+Disp energies are more repulsive than the TTM-nrg Pauli+Disp energies in $Li^+(H_2O)$ and $Na^+(H_2O)$, but are less repulsive in the other three dimers. Given that MB-nrg predicts 2B interaction energies that are on average the most consistent with the CCSD(T) reference 2B energies, it is clear that the PIPs provide accurate quantum corrections to the underlying long-range classical (TTM-nrg) potential.

4 Conclusions

We have analyzed the ability of (implict and explicit many-body) analytic PEFs as well as various XC functionals selected across the hierarchy of DFT approximations to describe alkali ion−water interactions through the decompositions of interaction energies calculated with each model into their fundamental physical contributions. Interaction energy decompositions

of the XC functionals have been carried out within the ALMO-EDA scheme. The accuracy of the various models at the 2B and 3B levels have been assessed through comparisons with the corresponding CCSD(T) reference energies. Our analysis indicates that analytic PEFs, which use simple classical representations of intermolecular interactions, are unable to correctly capture close-range effects such as charge transfer and Pauli repulsion. The decomposition of 2B energies predicted by XC functionals indicates that all models yield consistent polarization energies for all dimers, and consistent permanent electrostatic energies for all dimers except for $Li^+(H_2O)$, likely due to the small distance between Li^+ and the water-oxygen. We also find that the combined Pauli repulsion + Dispersion term is the most reflective of the differences between XC functionals (for all dimers except for $Li^+(H_2O)$) which was also found to be the case in halide−water interactions (note that Li^+ has no isoelectronic counterpart in the halides). Finally, comparisons between GGA and hybrid functionals, as well as comparisons between GGA and meta-GGA functionals in alkali ion−water and halide−water 2B ALMO-EDA, suggest that the differences in Pauli repulsion + Dispersion terms between functionals is a result of the delocalization error in GGA functionals, which leads to spurious Pauli repulsion, and the inability of functionals without dependence on the electronic kinetic energy density to reproduce intermediate-range dispersion interactions.

Supporting Information Available

Cartesian coordinates of low-lying isomers of $M^+(H_2O)$ and $M^+(H_2O)_2$ complexes, with M = Li, Na, K, Rb, and Cs, deviations of each tested model with respect to CCSD(T) for all $M^+(H_2O)_2$ complexes, 2B and 3B ALMO-EDA statistics for alkali ion−water interactions, and 2B ALMO-EDA statistics for halide−water interactions taken from J. Chem. Theory Comput. 2019, 15, 2983–2995.

Acknowledgement

This research was supported by the National Science Foundation through grant no. CHE-1453204. All calculations used resources of the Extreme Science and Engineering Discovery Environment (XSEDE),[92] which is supported by the National Science Foundation through grant no. ACI-1548562, under allocation TG-CHE110009, the High Performance Computing Modernization Program (HPCMP) through grant no. FA9550-16-1-0327 by the Air Force Office of Scientific Research, and the Triton Shared Computing Cluster (TSCC) at the San Diego Supercomputer Center.

References

(1) van Gunsteren, W. F.; Berendsen, H. J. C. Computer Simulation of Molecular Dynamics: Methodology, Applications, and Perspectives in Chemistry. *Angew. Chem., Int. Ed. Engl.* **1990**, *29*, 992–1023.

(2) Warshel, A. Computer Simulations of Enzyme Catalysis: Methods, Progress, and Insights. *Annu. Rev. Biophys. Biomol. Struct.* **2003**, *32*, 425–443.

(3) Garcia-Viloca, M.; Gao, J.; Karplus, M.; Truhlar, D. G. How Enzymes Work: Analysis by Modern Rate Theory and Computer Simulations. *Science* **2004**, *303*, 186–195.

(4) Yamakov, V.; Wolf, D.; Phillpot, S. R.; Mukherjee, A. K.; Gleiter, H. Deformation-Mechanism Map for Nanocrystalline Metals by Molecular-Dynamics Simulation. *Nat. Mater.* **2004**, *3*, 43.

(5) Nielsen, S. O.; Lopez, C. F.; Srinivas, G.; Klein, M. L. Coarse Grain Models and the Computer Simulation of Soft Materials. *J. Phys.: Condens. Matter* **2004**, *16*, R481.

(6) Markvoort, A. J.; Hilbers, P. A. J.; Nedea, S. V. Molecular Dynamics Study of the

Influence of Wall-Gas Interactions on Heat Flow in Nanochannels. *Phys. Rev. E* **2005**, *71*, 066702.

(7) Karplus, M.; Kuriyan, J. Molecular Dynamics and Protein Function. *Proc. Natl. Acad. Sci. U. S. A.* **2005**, *102*, 6679–6685.

(8) Voth, G. A. Computer Simulation of Proton Solvation and Transport in Aqueous and Biomolecular Systems. *Acc. Chem. Res.* **2006**, *39*, 143–150.

(9) De Vivo, M.; Masetti, M.; Bottegoni, G.; Cavalli, A. Role of Molecular Dynamics and Related Methods in Drug Discovery. *J. Med. Chem.* **2016**, *59*, 4035–4061.

(10) Tuckerman, M. *Statistical Mechanics: Theory and Molecular Simulation*; Oxford university press, 2010.

(11) Szabo, A.; Ostlund, N. S. *Modern Quantum Chemistry: Introduction to Advanced Electronic Structure Theory*; Courier Corporation, 2012.

(12) Bartlett, R. J.; Musiał, M. Coupled-Cluster Theory in Quantum Chemistry. *Rev. Mod. Phys.* **2007**, *79*, 291.

(13) Head-Gordon, M.; Artacho, E. Chemistry on the Computer. *Phys. Today* **2008**, *61*, 58.

(14) Mao, Y.; Demerdash, O.; Head-Gordon, M.; Head-Gordon, T. Assessing Ion–Water Interactions in the AMOEBA Force Field Using Energy Decomposition Analysis of Electronic Structure Calculations. *J. Chem. Theory Comput.* **2016**, *12*, 5422–5437.

(15) Schatz, G. C. The Analytical Representation of Electronic Potential-Energy Surfaces. *Rev. Mod. Phys.* **1989**, *61*, 669.

(16) Gillan, M. J.; Alfè, D.; Michaelides, A. Perspective: How Good is DFT for Water? *J. Chem. Phys.* **2016**, *144*, 130901.

(17) Cisneros, G. A.; Wikfeldt, K. T.; Ojamäe, L.; Lu, J.; Xu, Y.; Torabifard, H.; Bartók, A. P.; Csányi, G.; Molinero, V.; Paesani, F. Modeling Molecular Interactions in Water: From Pairwise to Many-Body Potential Energy Functions. *Chem. Rev.* **2016**, *116*, 7501–7528.

(18) Bajaj, P.; Götz, A. W.; Paesani, F. Toward Chemical Accuracy in the Description of Ion-Water Interactions Through Many-Body Representations. I. Halide-Water Dimer Potential Energy Surfaces. *J. Chem. Theory Comput.* **2016**, *12*, 2698–2705.

(19) Riera, M.; Mardirossian, N.; Bajaj, P.; Götz, A. W.; Paesani, F. Toward Chemical Accuracy in the Description of Ion–Water Interactions Through Many-Body Representations. Alkali-Water Dimer Potential Energy Surfaces. *J. Chem. Phys.* **2017**, *147*, 161715.

(20) Bizzarro, B. B.; Egan, C. K.; Paesani, F. Nature of Halide–Water Interactions: Insights from Many-Body Representations and Density Functional Theory. *J. Chem. Theory Comput.* **2019**, *15*, 2983–2995.

(21) Ren, P.; Ponder, J. W. Polarizable Atomic Multipole Water Model for Molecular Mechanics Simulation. *J. Phys. Chem. B* **2003**, *107*, 5933–5947.

(22) Ponder, J. W.; Wu, C.; Ren, P.; Pande, V. S.; Chodera, J. D.; Schnieders, M. J.; Haque, I.; Mobley, D. L.; Lambrecht, D. S.; DiStasio Jr, R. A.; ; Head-Gordon, M.; Clark, G. N. I.; Johnson, M. E.; Head-Gordon, T. Current Status of the AMOEBA Polarizable Force Field. *J. Phys. Chem. B* **2010**, *114*, 2549–2564.

(23) Arismendi-Arrieta, D. J.; Riera, M.; Bajaj, P.; Prosmiti, R.; Paesani, F. i-TTM Model for Ab Initio-Based Ion–Water Interaction Potentials. 1. Halide–Water Potential Energy Functions. *J. Phys. Chem. B* **2015**, *120*, 1822–1832.

(24) Riera, M.; Götz, A. W.; Paesani, F. The i-TTM model for Ab Initio-Based Ion–Water

Interaction Potentials. II. Alkali Metal Ion–Water Potential Energy Functions. *Phys. Chem. Chem. Phys.* **2016**, *18*, 30334–30343.

(25) Leach, A. R.; Leach, A. R. *Molecular Modelling: Principles and Applications*; Pearson education, 2001.

(26) Khaliullin, R. Z.; Cobar, E. A.; Lochan, R. C.; Bell, A. T.; Head-Gordon, M. Unravelling the Origin of Intermolecular Interactions Using Absolutely Localized Molecular Orbitals. *J. Phys. Chem. A* **2007**, *111*, 8753–8765.

(27) Horn, P. R.; Mao, Y.; Head-Gordon, M. Probing Non-Covalent Interactions with a Second Generation Energy Decomposition Analysis Using Absolutely Localized Molecular Orbitals. *Phys. Chem. Chem. Phys.* **2016**, *18*, 23067–23079.

(28) Horn, P. R.; Head-Gordon, M. Polarization Contributions to Intermolecular Interactions Revisited with Fragment Electric-Field Response Functions. *J. Chem. Phys.* **2015**, *143*, 114111.

(29) Horn, P. R.; Mao, Y.; Head-Gordon, M. Defining the Contributions of Permanent Electrostatics, Pauli Repulsion, and Dispersion in Density Functional Theory Calculations of Intermolecular Interaction Energies. *J. Chem. Phys.* **2016**, *144*, 114107.

(30) Mao, Y.; Ge, Q.; Horn, P. R.; Head-Gordon, M. On the Computational Characterization of Charge-Transfer Effects in Noncovalently Bound Molecular Complexes. *J. Chem. Theory Comput.* **2018**, *14*, 2401–2417.

(31) Phipps, M. J. S.; Fox, T.; Tautermann, C. S.; Skylaris, C.-K. Energy Decomposition Analysis Approaches and Their Evaluation on Prototypical Protein–Drug Interaction Patterns. *Chem. Soc. Rev.* **2015**, *44*, 3177–3211.

(32) Andres, J.; Ayers, P. W.; Boto, R. A.; Carbó-Dorca, R.; Chermette, H.; Cioslowski, J.; Contreras-García, J.; Cooper, D. L.; Frenking, G.; Gatti, C.; Heidar-Zadeh, F.; Jou-

bert, L.; Pendás, A. M.; Matito, E.; Mayer, I.; Misquitta, A. J.; Mo, Y.; Pilmé, J.; Popelier, P. L. A.; Rahm, M.; Ramos-Cordoba, E.; Salvador, P.; Schwarz, W. H. E.; Shahbazian, S.; Silvi, B.; Solà, M.; Szalewicz, K.; Tognetti, V.; Weinhold, F.; Zins, E.-L. Nine Questions on Energy Decomposition Analysis. *J. Comput. Chem* **2019**, *40*, 2248–2283.

(33) Braams, B. J.; Bowman, J. M. Permutationally Invariant Potential Energy Surfaces in High Dimensionality. *Int. Rev. Phys. Chem.* **2009**, *28*, 577–606.

(34) Purvis III, G. D.; Bartlett, R. J. A Full Coupled-Cluster Singles and Doubles Model: The Inclusion of Disconnected Triples. *J. Chem. Phys.* **1982**, *76*, 1910–1918.

(35) Raghavachari, K.; Trucks, G. W.; Pople, J. A.; Head-Gordon, M. A Fifth-Order Perturbation Comparison of Electron Correlation Theories. *Chem. Phys. Lett* **1989**, *157*, 479–483.

(36) Perdew, J. P.; Parr, R. G.; Levy, M.; Balduz Jr, J. L. Density-functional theory for fractional particle number: derivative discontinuities of the energy. *Phys. Rev. Lett.* **1982**, *49*, 1691.

(37) Mori-Sánchez, P.; Cohen, A. J.; Yang, W. Many-Electron Self-Interaction Error in Approximate Density Functionals. *J. Chem. Phys.* **2006**, *125*, 201102.

(38) Hait, D.; Head-Gordon, M. Delocalization Errors in Density Functional Theory Are Essentially Quadratic in Fractional Occupation Number. *J. Phys. Chem. Lett.* **2018**, *9*, 6280–6288.

(39) Møller, C.; Plesset, M. S. Note on an Approximation Treatment for Many-Electron Systems. *Phys. Rev.* **1934**, *46*, 618.

(40) El Azhary, A.; Rauhut, G.; Pulay, P.; Werner, H.-J. Analytical Energy Gradients for

Local Second-Order Møller–Plesset Perturbation Theory. *J. Chem. Phys.* **1998**, *108*, 5185–5193.

(41) Dunning Jr, T. H. Gaussian Basis Sets for Use in Correlated Molecular Calculations. I. The Atoms Boron Through Neon and Hydrogen. *J. Chem. Phys.* **1989**, *90*, 1007–1023.

(42) Kendall, R. A.; Dunning Jr, T. H.; Harrison, R. J. Electron Affinities of the First-Row Atoms Revisited. Systematic Basis Sets and Wave Functions. *J. Chem. Phys.* **1992**, *96*, 6796–6806.

(43) Prascher, B. P.; Woon, D. E.; Peterson, K. A.; Dunning, T. H.; Wilson, A. K. Gaussian Basis Sets for Use in Correlated Molecular Calculations. VII. Valence, Core-Valence, and Scalar Relativistic Basis Sets for Li, Be, Na, and Mg. *Theor. Chem. Acc.* **2011**, *128*, 69–82.

(44) Hill, J. G.; Peterson, K. A. Gaussian Basis Sets for Use in Correlated Molecular Calculations. XI. Pseudopotential-Based and All-Electron Relativistic Basis Sets for Alkali Metal (K–Fr) and Alkaline Earth (Ca–Ra) Elements. *J. Chem. Phys.* **2017**, *147*, 244106.

(45) Lim, I. S.; Schwerdtfeger, P.; Metz, B.; Stoll, H. All-Electron and Relativistic Pseudopotential Studies for the Group 1 Element Polarizabilities from K to Element 119. *J. Chem. Phys.* **2005**, *122*, 104103.

(46) Feyereisen, M.; Fitzgerald, G.; Komornicki, A. Use of Approximate Integrals in Ab Initio Theory. An Application in MP2 Energy Calculations. *Chem. Phys. Lett.* **1993**, *208*, 359–363.

(47) Weigend, F.; Häser, M. RI-MP2: First Derivatives and Global Consistency. *Theor. Chem. Acc.* **1997**, *97*, 331–340.

(48) Góra, U.; Podeszwa, R.; Cencek, W.; Szalewicz, K. Interaction Energies of Large Clusters from Many-Body Expansion. *J. Chem. Phys.* **2011**, *135*, 224102.

(49) Werner, H.-J.; Knowles, P. J.; Knizia, G.; Manby, F. R.; Schütz, M.; Celani, P.; Györffy, W.; Kats, D.; Korona, T.; Lindh, R.; Mitrushenkov, A.; Rauhut, G.; Shamasundar, K. R.; Adler, T. B.; Amos, R. D.; Bernhardsson, A.; Berning, A.; Cooper, D. L.; Deegan, M. J.; Dobbyn, A. J.; Eckert, F.; Goll, E.; Hampel, C.; Hesselmann, A.; Hetzer, G.; Hrenar, T.; Jansen, G.; Köppl, C.; Liu, Y.; Lloyd, A. W.; Mata, R. A.; May, A. J.; McNicholas, S. J.; Meyer, W.; Mura, M. E.; Nicklass, A.; O'Neill, D. P.; Palmieri, P.; Peng, D.; Pflüger, K.; Pitzer, R.; Reiher, M.; Shiozaki, T.; Stoll, H.; Stone, A. J.; Tarroni, R.; Thorsteinsson, T.; Wang, M. *MOLPRO, a Package of Ab Initio Programs*, version 2015.1 ed.; 2015; see http://www.molpro.net.

(50) Grossfield, A.; Ren, P.; Ponder, J. W. Ion Solvation Thermodynamics from Simulation with a Polarizable Force Field. *J. Am. Chem. Soc.* **2003**, *125*, 15671–15682.

(51) Ren, P.; Ponder, J. W. Temperature and Pressure Dependence of the AMOEBA Water Model. *J. Phys. Chem. B* **2004**, *108*, 13427–13437.

(52) Wu, J. C.; Chattree, G.; Ren, P. Automation of AMOEBA Polarizable Force Field Parameterization for Small Molecules. *Theor. Chem. Acc.* **2012**, *131*, 1138.

(53) Wang, L.-P.; Head-Gordon, T.; Ponder, J. W.; Ren, P.; Chodera, J. D.; Eastman, P. K.; Martinez, T. J.; Pande, V. S. Systematic Improvement of a Classical Molecular Model of Water. *J. Phys. Chem. B* **2013**, *117*, 9956–9972.

(54) Thole, B. T. Molecular Polarizabilities Calculated with a Modified Dipole Interaction. *Chem. Phys.* **1981**, *59*, 341–350.

(55) Halgren, T. A. The Representation of van der Waals (vdW) Interactions in Molecular Mechanics Force Fields: Potential Form, Combination Rules, and vdW Parameters. *J. Am. Chem. Soc.* **1992**, *114*, 7827–7843.

(56) Babin, V.; Leforestier, C.; Paesani, F. Development of a "First Principles" Water Po-

tential with Flexible Monomers: Dimer Potential Energy Surface, VRT Spectrum, and Second Virial Coefficient. *J. Chem. Theory Comput.* **2013**, *9*, 5395–5403.

(57) Medders, G. R.; Babin, V.; Paesani, F. A Critical Assessment of Two-Body and Three-Body Interactions in Water. *J. Chem. Theory Comput.* **2013**, *9*, 1103–1114.

(58) Medders, G. R.; Paesani, F. Many-Body Convergence of the Electrostatic Properties of Water. *J. Chem. Theory Comput.* **2013**, *9*, 4844–4852.

(59) Babin, V.; Medders, G. R.; Paesani, F. Development of a "First Principles" Water Potential with Flexible Monomers. II: Trimer Potential Energy Surface, Third Virial Coefficient, and Small Clusters. *J. Chem. Theory Comput.* **2014**, *10*, 1599–1607.

(60) Medders, G. R.; Babin, V.; Paesani, F. Development of a "First-Principles" Water Potential with Flexible Monomers. III. Liquid Phase Properties. *J. Chem. Theory Comput.* **2014**, *10*, 2906–2910.

(61) Becke, A. D.; Johnson, E. R. Exchange-Hole Dipole Moment and the Dispersion Interaction. *J. Chem. Phys.* **2005**, *122*, 154104.

(62) Johnson, E. R.; Becke, A. D. A Post-Hartree–Fock Model of Intermolecular Interactions. *J. Chem. Phys.* **2005**, *123*, 024101.

(63) Johnson, E. R.; Becke, A. D. A Post-Hartree-Fock Model of Intermolecular Interactions: Inclusion of Higher-Order Corrections. *J. Chem. Phys.* **2006**, *124*, 174104.

(64) Kannemann, F. O.; Becke, A. D. Van der Waals Interactions in Density-Functional Theory: Intermolecular Complexes. *J. Chem. Theory Comput.* **2010**, *6*, 1081–1088.

(65) Otero-De-La-Roza, A.; Johnson, E. R. Non-Covalent Interactions and Thermochemistry Using XDM-Corrected Hybrid and Range-Separated Hybrid Density Functionals. *J. Chem. Phys.* **2013**, *138*, 204109.

(66) Tang, K. T.; Toennies, J. P. An Improved Simple Model for the van der Waals Potential Based on Universal Damping Functions for the Dispersion Coefficients. *J. Chem. Phys.* **1984**, *80*, 3726–3741.

(67) Hankins, D.; Moskowitz, J.; Stillinger, F. Water Molecule Interactions. *J. Chem. Phys.* **1970**, *53*, 4544–4554.

(68) Tikhonov, A. N. Solution of Incorrectly Formulated Problems and the Regularization Method. Soviet Math. Dokl. 1963; pp 1035–1038.

(69) Adler, T. B.; Knizia, G.; Werner, H. J. A Simple and Efficient CCSD(T)-F12 Approximation. *J. Chem. Phys.* **2007**, *127*, 221106.

(70) Knizia, G.; Adler, T. B.; Werner, H. J. Simplified CCSD(T)-F12 Methods: Theory and Benchmarks. *J. Chem. Phys.* **2009**, *130*, 054104.

(71) Becke, A. D. Density-Functional Exchange-Energy Approximation with Correct Asymptotic Behavior. *Phys. Rev. A* **1988**, *38*, 3098.

(72) Lee, C.; Yang, W.; Parr, R. G. Development of the Colle-Salvetti Correlation-Energy Formula into a Functional of the Electron Density. *Phys. Rev. B* **1988**, *37*, 785.

(73) Perdew, J. P.; Burke, K.; Ernzerhof, M. Generalized Gradient Approximation Made Simple. *Phys. Rev. Lett.* **1996**, *77*, 3865.

(74) Zhang, Y.; Yang, W. Comment on "Generalized Gradient Approximation Made Simple". *Phys. Rev. Lett.* **1998**, *80*, 890.

(75) Sun, J.; Ruzsinszky, A.; Perdew, J. P. Strongly Constrained and Appropriately Normed Semilocal Density Functional. *Phys. Rev. Lett* **2015**, *115*, 036402.

(76) Tao, J.; Perdew, J. P.; Staroverov, V. N.; Scuseria, G. E. Climbing the Density Functional Ladder: Nonempirical Meta–Generalized Gradient Approximation Designed for Molecules and Solids. *Phys. Rev. Lett.* **2003**, *91*, 146401.

(77) Mardirossian, N.; Head-Gordon, M. Mapping the Genome of Meta-Generalized Gradient Approximation Density Functionals: The Search for B97M-V. *J. Chem. Phys.* **2015**, *142*, 074111.

(78) Mardirossian, N.; Ruiz Pestana, L.; Womack, J. C.; Skylaris, C.-K.; Head-Gordon, T.; Head-Gordon, M. Use of the rVV10 Nonlocal Correlation Functional in the B97M-V Density Functional: Defining B97M-rV and Related Functionals. *J. Phys. Chem. Lett* **2016**, *8*, 35–40.

(79) Becke, A. D. Density-Functional Thermochemistry. III. The Role of Exact Exchange. *J. Chem. Phys.* **1993**, *98*, 5648–5652.

(80) Adamo, C.; Barone, V. Toward Reliable Density Functional Methods Without Adjustable Parameters: The PBE0 Model. *J. Chem. Phys.* **1999**, *110*, 6158–6170.

(81) Zhao, Y.; Truhlar, D. G. The M06 Suite of Density Functionals for Main Group Thermochemistry, Thermochemical Kinetics, Noncovalent Interactions, Excited States, and Transition Elements: Two New Functionals and Systematic Testing of Four M06-Class Functionals and 12 Other Functionals. *Theor. Chem. Acc.* **2008**, *120*, 215–241.

(82) Chai, J.-D.; Head-Gordon, M. Systematic Optimization of Long-Range Corrected Hybrid Density Functionals. *J. Chem. Phys.* **2008**, *128*, 084106.

(83) Mardirossian, N.; Head-Gordon, M. ω B97M-V: A Combinatorially Optimized, Range-Separated Hybrid, Meta-GGA Density Functional with VV10 Nonlocal Correlation. *J. Chem. Phys.* **2016**, *144*, 214110.

(84) Grimme, S.; Antony, J.; Ehrlich, S.; Krieg, H. A Consistent and Accurate Ab Initio Parametrization of Density Functional Dispersion Correction (DFT-D) for the 94 Elements H-Pu. *J. Chem. Phys.* **2010**, *132*, 154104.

(85) Chai, J.-D.; Head-Gordon, M. Long-Range Corrected Hybrid Density Functionals with Damped Atom–Atom Dispersion Corrections. *Phys. Chem. Chem. Phys.* **2008**, *10*, 6615–6620.

(86) Shao, Y.; Gan, Z.; Epifanovsky, E.; Gilbert, A. T. B.; Wormit, M.; Kussmann, J.; Lange, A. W.; Behn, A.; Deng, J.; Feng, X.; Ghosh, D.; Goldey, M.; Horn, P. R.; Jacobson, L. D.; Kaliman, I.; Khaliullin, R. Z.; Kús, T.; Landau, A.; Liu, J.; Proynov, E. I.; Rhee, Y. M.; Richard, R. M.; Rohrdanz, M. A.; Steele, R. P.; Sundstrom, E. J.; Woodcock III, H. L.; Zimmerman, P. M.; Zuev, D.; Albrecht, B.; Alguire, E.; Austin, B.; Beran, G. J. O.; Bernard, Y. A.; Berquist, E.; Brandhorst, K.; Bravaya, K. B.; Brown, S. T.; Casanova, D.; Chang, C.-M.; Chen, Y.; Chien, S. H.; Closser, K. D.; Crittenden, D. L.; Diedenhofen, M.; DiStasio Jr., R. A.; Dop, H.; Dutoi, A. D.; Edgar, R. G.; Fatehi, S.; Fusti-Molnar, L.; Ghysels, A.; Golubeva-Zadorozhnaya, A.; Gomes, J.; Hanson-Heine, M. W. D.; Harbach, P. H. P.; Hauser, A. W.; Hohenstein, E. G.; Holden, Z. C.; Jagau, T.-C.; Ji, H.; Kaduk, B.; Khistyaev, K.; Kim, J.; Kim, J.; King, R. A.; Klunzinger, P.; Kosenkov, D.; Kowalczyk, T.; Krauter, C. M.; Lao, K. U.; Laurent, A.; Lawler, K. V.; Levchenko, S. V.; Lin, C. Y.; Liu, F.; Livshits, E.; Lochan, R. C.; Luenser, A.; Manohar, P.; Manzer, S. F.; Mao, S.-P.; Mardirossian, N.; Marenich, A. V.; Maurer, S. A.; Mayhall, N. J.; Oana, C. M.; Olivares-Amaya, R.; O'Neill, D. P.; Parkhill, J. A.; Perrine, T. M.; Peverati, R.; Pieniazek, P. A.; Prociuk, A.; Rehn, D. R.; Rosta, E.; Russ, N. J.; Sergueev, N.; Sharada, S. M.; Sharmaa, S.; Small, D. W.; Sodt, A.; Stein, T.; Stück, D.; Su, Y.-C.; Thom, A. J. W.; Tsuchimochi, T.; Vogt, L.; Vydrov, O.; Wang, T.; Watson, M. A.; Wenzel, J.; White, A.; Williams, C. F.; Vanovschi, V.; Yeganeh, S.; Yost, S. R.; You, Z.-Q.; Zhang, I. Y.; Zhang, X.; Zhou, Y.; Brooks, B. R.; Chan, G. K. L.; Chipman, D. M.; Cramer, C. J.; Goddard III, W. A.; Gordon, M. S.; Hehre, W. J.; Klamt, A.; Schaefer III, H. F.; Schmidt, M. W.; Sherrill, C. D.; Truhlar, D. G.; Warshel, A.; Xua, X.; Aspuru-Guzik, A.; Baer, R.; Bell, A. T.; Besley, N. A.; Chai, J.-D.; Dreuw, A.; Dunietz, B. D.;

Furlani, T. R.; Gwaltney, S. R.; Hsu, C.-P.; Jung, Y.; Kong, J.; Lambrecht, D. S.; Liang, W.; Ochsenfeld, C.; Rassolov, V. A.; Slipchenko, L. V.; Subotnik, J. E.; Van Voorhis, T.; Herbert, J. M.; Krylov, A. I.; Gill, P. M. W.; Head-Gordon, M. Advances in Molecular Quantum Chemistry Contained in the Q-Chem 4 Program Package. *Mol. Phys.* **2015**, *113*, 184–215.

(87) Jensen, F. Describing Anions by Density Functional Theory: Fractional Electron Affinity. *J. Chem. Theory Comput.* **2010**, *6*, 2726–2735.

(88) Kristyán, S.; Pulay, P. Can (Semi) Local Density Functional Theory Account for the London Dispersion Forces? *Chem. Phys. Lett* **1994**, *229*, 175–180.

(89) Sun, J.; Remsing, R. C.; Zhang, Y.; Sun, Z.; Ruzsinszky, A.; Peng, H.; Yang, Z.; Paul, A.; Waghmare, U.; Wu, X.; Klein, M. L. K.; Perdew, J. P. Accurate First-Principles Structures and Energies of Diversely Bonded Systems from an Efficient Density Functional. *Nat. Chem* **2016**, *8*, 831.

(90) Sabatini, R.; Gorni, T.; De Gironcoli, S. Nonlocal van der Waals Density Functional Made Simple and Efficient. *Phys. Rev. B* **2013**, *87*, 041108.

(91) Grimme, S. Density Functional Theory with London Dispersion Corrections. *Wiley Interdiscip. Rev. Comput. Mol. Sci* **2011**, *1*, 211–228.

(92) Towns, J.; Cockerill, T.; Dahan, M.; Foster, I.; Gaither, K.; Grimshaw, A.; Hazlewood, V.; Lathrop, S.; Lifka, D.; Peterson, G. D.; Roskies, R.; Scott, J. R.; Wilkins-Diehr, N. XSEDE: Accelerating Scientific Discovery. *Comput. Sci. Eng.* **2014**, *16*, 62–74.

TOC Figure

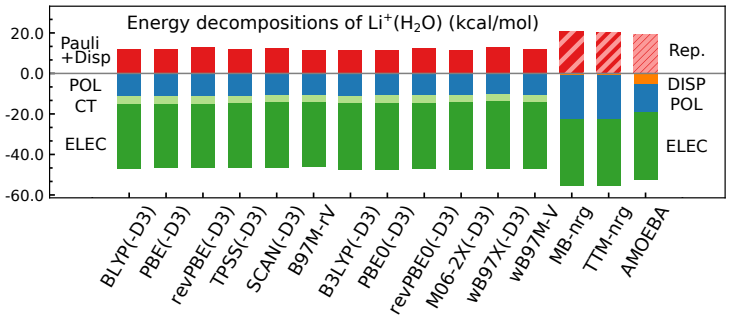
Energy decompositions of Li+(H2O) (kcal/mol)
20.0
0.0
-20.0
-40.0
-60.0
Pauli
+Disp
POL
CT
ELEC
Rep.
DISP
POL
ELEC
BLYP(-D3)
PBE(-D3)
revPBE(-D3)
TPSS(-D3)
SCAN(-D3)
B97M-rV
B3LYP(-D3)
PBE0(-D3)
revPBE0(-D3)
M06-2X(-D3)
wB97X(-D3)
wB97M-V
MB-nrg
TTM-nrg
AMOEBA